Article

Immunity

Class-Switch Recombination Occurs Infrequently in Germinal Centers

Graphical Abstract

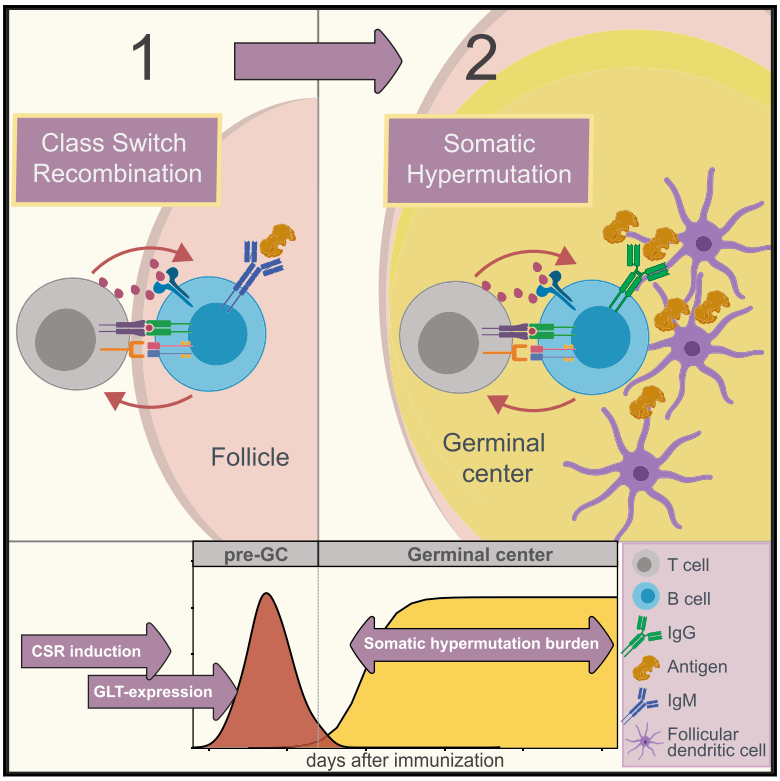

Highlights

- Germline transcripts peak prior to GC formation and rapidly decline in GCs
- IgM-dominated clones are found in late GCs, arguing against ongoing Ig switching
- CSR largely ceases upon the onset of somatic hypermutation
- CSR decline due to low GLT and APE1 expression is possibly orchestrated by BCL6

Authors

Jonathan A. Roco, Luka Mesin, Sebastian C. Binder, ..., Michael Meyer-Hermann, Gabriel D. Victora, Carola G. Vinuesa

Correspondence

carola.vinuesa@anu.edu.au

In Brief

Germinal centers (GCs) have long been considered sites in which Ig class-switch recombination (CSR) is favored. Roco et al. show that CSR occurs during the initial T cell:B cell interaction prior to GC formation and rapidly declines as B cells differentiate into GC cells and somatic hypermutation commences.

Roco et al., 2019, Immunity *51*, 337–350
August 20, 2019
https://doi.org/10.1016/j.immuni.2019.07.001

CellPress

Immunity
Article

Class-Switch Recombination Occurs Infrequently in Germinal Centers

Jonathan A. Roco,[1] Luka Mesin,[2] Sebastian C. Binder,[3] Christian Nefzger,[5] Paula Gonzalez-Figueroa,[1] Pablo F. Canete,[1] Julia Ellyard,[1] Qian Shen,[1] Philippe A. Robert,[3] Jean Cappello,[1] Harpreet Vohra,[1] Yang Zhang,[6] Carla R. Nowosad,[2] Arien Schiepers,[2] Lynn M. Corcoran,[7,8] Kai-Michael Toellner,[6] Jose M. Polo,[5] Michael Meyer-Hermann,[3,4] Gabriel D. Victora,[2] and Carola G. Vinuesa[1,9,10,*]

[1]Department of Immunology and Infectious Disease and Centre for Personalised Immunology, The John Curtin School of Medical Research, The Australian National University, Canberra ACT 0200, Australia
[2]Laboratory of Lymphocyte Dynamics, Rockefeller University, New York, NY, 10065, USA
[3]Department of Systems Immunology and Braunschweig Integrated Centre of Systems Biology, Helmholtz Centre for Infection Research, Rebenring 56, 38106 Braunschweig, Germany
[4]Institute for Biochemistry, Biotechnology, and Bioinformatics, Technische Universität Braunschweig, Braunschweig, Germany
[5]Department of Anatomy and Developmental Biology and Australian Regenerative Medicine Institute, Monash University, Wellington Road, Clayton VIC 3800, Australia
[6]Institute of Immunology and Immunotherapy, University of Birmingham, Birmingham B15 2TT, UK
[7]Molecular Immunology Division, the Walter and Eliza Hall Institute of Medical Research, Parkville, Victoria, Australia
[8]Department of Medical Biology, The University of Melbourne, Parkville VIC 3052, Australia
[9]China-Australia Centre for Personalised Immunology, Department of Rheumatology, Shanghai Renji Hospital, Shanghai JiaoTong University, Shanghai, China
[10]Lead Contact
*Correspondence: carola.vinuesa@anu.edu.au
https://doi.org/10.1016/j.immuni.2019.07.001

SUMMARY

Class-switch recombination (CSR) is a DNA recombination process that replaces the immunoglobulin (Ig) constant region for the isotype that can best protect against the pathogen. Dysregulation of CSR can cause self-reactive BCRs and B cell lymphomas; understanding the timing and location of CSR is therefore important. Although CSR commences upon T cell priming, it is generally considered a hallmark of germinal centers (GCs). Here, we have used multiple approaches to show that CSR is triggered prior to differentiation into GC B cells or plasmablasts and is greatly diminished in GCs. Despite finding a small percentage of GC B cells expressing germline transcripts, phylogenetic trees of GC BCRs from secondary lymphoid organs revealed that the vast majority of CSR events occurred prior to the onset of somatic hypermutation. As such, we have demonstrated the existence of IgM-dominated GCs, which are unlikely to occur under the assumption of ongoing switching.

INTRODUCTION

Class-switch recombination (CSR) is an intrachromosomal DNA rearrangement of the immunoglobulin (Ig) heavy-chain locus. As a result, IgM-IgD mature B cells are able to express antibodies of the IgA, IgG, or IgE classes that differ in effector functions without altering the specificity for the immunizing antigen (Stavnezer et al., 2008). CSR relies primarily on activation of the enzymes Activation induced cytidine deaminase (AID), uracil-DNA glycosylase (UNG), and apurinic-apyrimidinic endonuclease 1 (APE1) to specifically target intronic areas called switch (S) regions (Guikema et al., 2007; Muramatsu et al., 2000; Rada et al., 2002). DNA breaks introduced by these enzymes lead to the recombination of the variable heavy-chain (VDJ) segment with a different constant heavy (C_H) chain gene (isotype) (Stavnezer et al., 2008). Selection of the appropriate isotype during infection is driven by cytokines and T cell help (Kawabe et al., 1994; Snapper and Mond, 1993), which induce transcription across the specific S regions with production of germline transcripts (GLTs) (Lorenz et al., 1995). GLTs (also known as switch transcripts) are spliced, polyadenylated non-coding mRNAs transcribed from specific promoters located upstream of each set of S regions (except for IgD). Expression of GLTs precedes DNA recombination of the Ig-C_H genes in B cells primed to undergo CSR (Stavnezer, 1996). For this reason, GLTs have long been used as a reliable molecular marker to study the onset of CSR *in vivo* (Cogné and Birshtein, 2004; Lorenz et al., 1995).

Germinal centers (GCs) are specialized microenvironments in secondary lymphoid organs formed upon immunization. GCs are critical for the formation of long-lived plasma cells and memory B cells. Within these structures, B cells undergo somatic hypermutation (SHM) and clonal selection based on the affinity of the B cell receptor (BCR) for the immunizing antigen. Likewise, GCs are also considered to be the main areas where CSR takes place (Klein and Dalla-Favera, 2008; Vinuesa et al., 2009). Although SHM and CSR are two independent processes, both depend on the activity of AID (Muramatsu et al., 2000), which is expressed at highest amounts in GC B cells. These observations might have reinforced the idea that CSR is predominantly a GC process.

CSR has been typically studied using *in vitro* culture systems or after clonal expansion of B cells *in vivo*. In these studies, an important role of the GC environment in CSR has been postulated after finding GLTs are predominantly

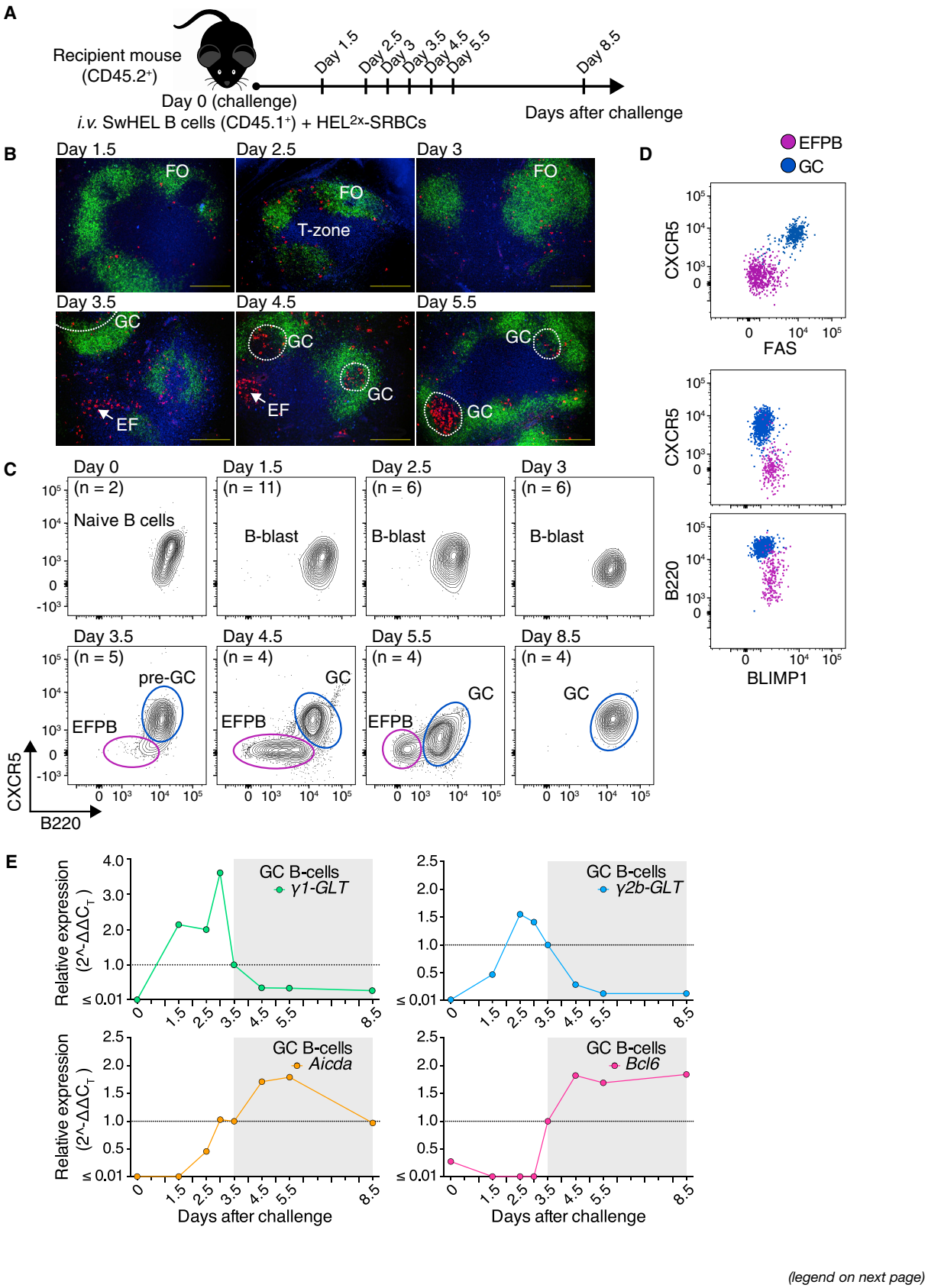

(legend on next page)

expressed by human cells bearing centrocyte-specific markers, such as CD77 (Liu et al., 1996). However, these markers have been later shown to also identify activated B cells and plasmablasts (Högerkorp and Borrebaeck, 2006). The association between CSR and GCs also comes from studies in genetically manipulated mice with impaired formation of follicular structures that are likely to also perturb early T cell:B cell encounters (Shinkura et al., 1996). Nevertheless, extrafollicular (EF) responses are known to produce switched antibodies, and induction of CSR has been detected as early as day 2 during a primary immune response (Cerutti, 2008; Fagarasan et al., 2001; Jacob et al., 1991; Pape et al., 2003; Toellner et al., 1996). Despite this evidence, it is still generally believed that isotype switching is an ongoing process that continues and is enhanced within GCs.

Here, we used transgenic mouse models that allow us to unequivocally distinguish GC B cells, EF plasmablasts (EFPBs), and their precursors from the earliest stages of an immune response *in vivo*. We show that CSR is initiated over the first few days in a primary response and prior to EF and GC commitment, ceasing soon after B cells become GC cells and SHM commences. We also demonstrate the existence of IgM-dominated GCs, which are unlikely to occur under the assumption of ongoing switching.

RESULTS

GLT Expression Is Triggered at the Early Stages of B Cell Activation and Rapidly Declines within GCs

In order to identify the cells in which CSR is first triggered, we took advantage of SW_{HEL} mice, in which 5%–15% of the B cells carry a high-affinity BCR against hen egg lysozyme (HEL) (Phan et al., 2003). We adoptively transferred 3–15 × 10^4 SW_{HEL} B cells into C57BL/6 mice along with mutated HEL ($HEL^{2\times}$) protein conjugated to sheep red blood cells (SRBCs) (Figure 1A). SW_{HEL} B cells bind $HEL^{2\times}$ with moderate affinity and undergo CSR and SHM normally (Paus et al., 2006). Practically, all transferred B cells are known to be recruited into the response (Chan et al., 2009). As described in these previous studies, upon HEL-SRBC immunization, adoptively transferred SW_{HEL} B cells first appeared at the T cell:B cell border on day 1.5, at the periphery of the follicles on day 2.5, and within primary follicles on day 3 (Figure 1B). On day 3.5, HEL-binding B cells were found forming nascent GCs, and HEL-binding EFPBs were also seen (Figure 1B). A homogeneous B cell population was observed by flow cytometry up to day 3 (Figure 1C). Consistent with the immunofluorescence findings, day 3.5 marked the appearance of GC B cells and EFPBs by flow cytometry. EFPBs were distinguished by downregulation of the chemokine receptor CXCR5, as well as B220 (Figure 1C), shown to occur as B cells express BLIMP1 (Figures 1D, S1A, and S1B) and localize to extrafollicular foci (Chan et al., 2009). GC B cells seen at day 3.5 remained $CXCR5^{hi}$ $B220^{hi}$ (Figure 1C) and also expressed FAS death receptor (Figure S1A). These populations were sorted at 12- to 24-h intervals from day 1.5 after immunization, and *γ1* and *γ2b-GLTs*, the most abundant isotypes in the SRBC response (Phan et al., 2005), were quantified by qPCR. GLTs were first seen at day 1.5, peaked at days 2.5–3 prior to GC formation, and declined rapidly thereafter to become barely detectable 48 h later (Figure 1E). Of note, total RNA amounts used for PCR amplification and RNA quality were comparable throughout the time course (Figure S2A). *Aicda* mRNA (encoding AID) was first detected at day 2.5, 12 h after production of the first GLT and 24 h prior to the appearance of EFPB or GC (Figure 1E). Expression of *Bcl6*, the transcription factor required for GC B cell differentiation, was first detected at day 3.5 (Figure 1E). Thus, CSR is triggered prior to EF or GC B cell commitment, and GLTs decline prior to GC formation.

Class-Switched Antibodies Are Detected Prior to GC Formation and Are Comparable within GCs and EFPBs

We next compared the production of surface IgG in GCs and EF foci (Figures 2A–2D). Class-switched B cells first appeared at day 2.5, one day after detection of the first GLT (Figure 2B), coinciding with the earliest detection of *Aicda* mRNA (Figure 1E). IgG^+ cells increased exponentially over the following two days, reaching a plateau from days 4.5–6.5 with approximately 70% of GC B cells and 90% of EFPBs having switched (Figures 2C, 2D, and S2B). The paucity of IgM^+ EFPBs at this time point may be due to the greater proliferative ability of switched cells (Martin and Goodnow, 2002; Tangye et al., 2003).

The affinity of SW_{HEL} B cells for $HEL^{2\times}$ is still quite high (8 × 10^7 M^{-1}), and there is some evidence that signal strength may play a role in driving early B cell events (Chan et al., 2009; Paus et al., 2006). To exclude the possibility that strong and uniform early switching may have been driven by affinity, we repeated the experiments using $HEL^{3\times}$, which carries an additional mutation that further lowers the affinity of the SW_{HEL} BCR interaction to 1.5 × 10^6 M^{-1} (Paus et al., 2006). We observed a small delay in the formation of GCs using $HEL^{3\times}$; at day 3.5, HEL-binding B cells still appeared as a single population of activated B cells that hadn't yet become GC cells (Figure S2C). As seen with $HEL^{2\times}$, *γ1-GLT* peaked at this pre-GC stage, and a dramatic decline in GLTs was seen at the peak of the GC reaction (Figures S2D and S2E). These results confirm that early and rapidly declining switching is a reproducible finding.

Figure 1. Isotype Switching Commences Prior to GC Onset

(A) Adoptive transfer protocol of SW_{HEL} B cells and $HEL^{2\times}$-SRBCs into congenic recipient mice (see STAR Methods).

(B) Immunofluorescence images of spleen sections collected from recipient mice as in (A). Sections were stained for SW_{HEL} B cells (red), IgD (green), and CD3 (blue). Scale bars are 200 μm.

(C and D) Representative flow-cytometric plots showing gating strategy to identify donor-derived Sw_{HEL} B cells after adoptive transfer (C) and expression (D) of BLIMP1 versus CXCR5 or B220 and FAS versus CXCR5 in HEL-binding B cells recovered 5 days after challenge as shown in (A).

(E) qPCR gene-expression profile of purified donor-derived SW_{HEL} B cells for *γ1-GLT*, *γ2b-GLT*, *Aicda*, and *Bcl6*. Data were normalized to the reference gene *Ubc* and is presented as a fold change compared to day 3.5 values using the $\Delta\Delta C_T$ method. Dots represent the mean of pooled biological replicates as in (C). Data are representative of two independent experiments. n = number of recipient mice used at each time point. See also Figures S1 and S2.

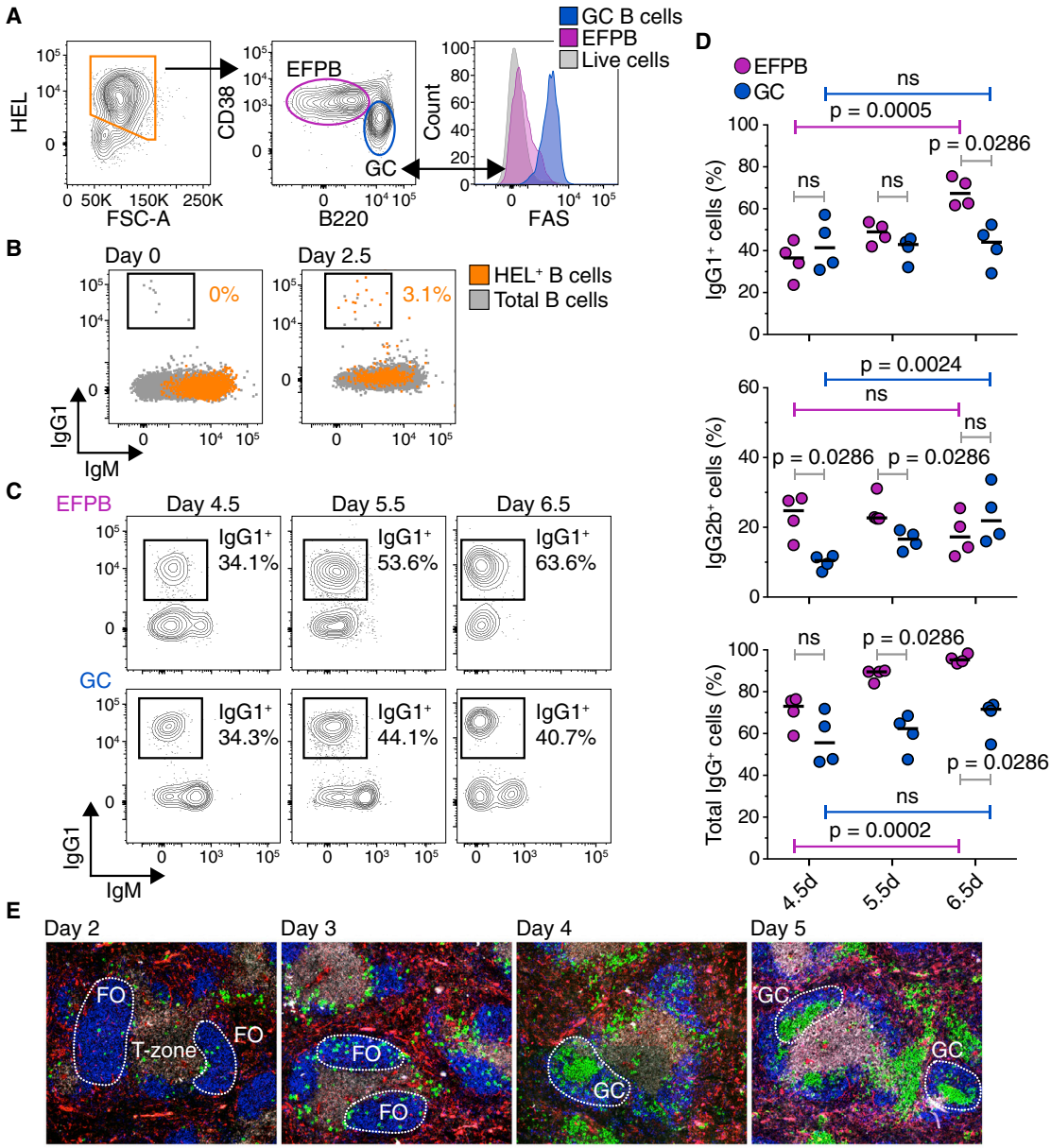

Figure 2. Class Switching Proceeds at Comparable Rates in GCs and EF Sites and Early Visualization of Germline Transcription in a Polyclonal Response

(A) Flow-cytometric plots showing gating strategy employed to identify donor-derived SW_{HEL} B cells after immunization as shown in Figure 1.

(B and C) Flow-cytometric analysis for surface expression of IgG1 and IgM in naive (day 0), activated (day 2.5) (B), EFPB, and GC SW_{HEL} B cells (days 4.5–6.5) (C). Numbers indicate the percentage of donor-derived HEL^+ $IgG1^+$ cells.

(D) Quantification of IgG1, IgG2b, and total IgG in EFPBs and GC B cells as shown in (C). Bars represent medians and dots represent individual mice (n = 4). Horizontal gray bars show comparisons between EFPB and GC subsets at the same time point (Mann-Whitney U test). Horizontal purple and blue bars show comparisons between EFPBs or GC B cells (Kruskal-Wallis test), respectively. Numbers on top of bars indicate the respective p value. ns, not significant.

(E) Immunofluorescence images of spleen sections from Cγ1-Cre:mT/mG mice after SRBC immunization at the indicated time points: CD3 (gray), IgD (blue), Cγ1-Cre (green), and non-activated B cells (red).

Data are representative of two (A–D) and three (E) independent experiments. See also Figure S2.

Germline Transcription Is Rapidly Induced at the T Cell:B Cell Border

We next sought to visualize the precise location in which isotype switching was initiated in C57BL/6 mice with a polyclonal BCR repertoire. For this, we used Cγ1-Cre:mT/mG mice (Casola et al., 2006; Muzumdar et al., 2007), in which production of the *γ1-GLT* can be tracked by GFP expression. After SRBC immunization, the first GFP^+ cells were detected on day 2 and were found predominantly at the T cell:B cell border (Figure 2E). By day 3, GFP^+ cells had expanded and could be found within

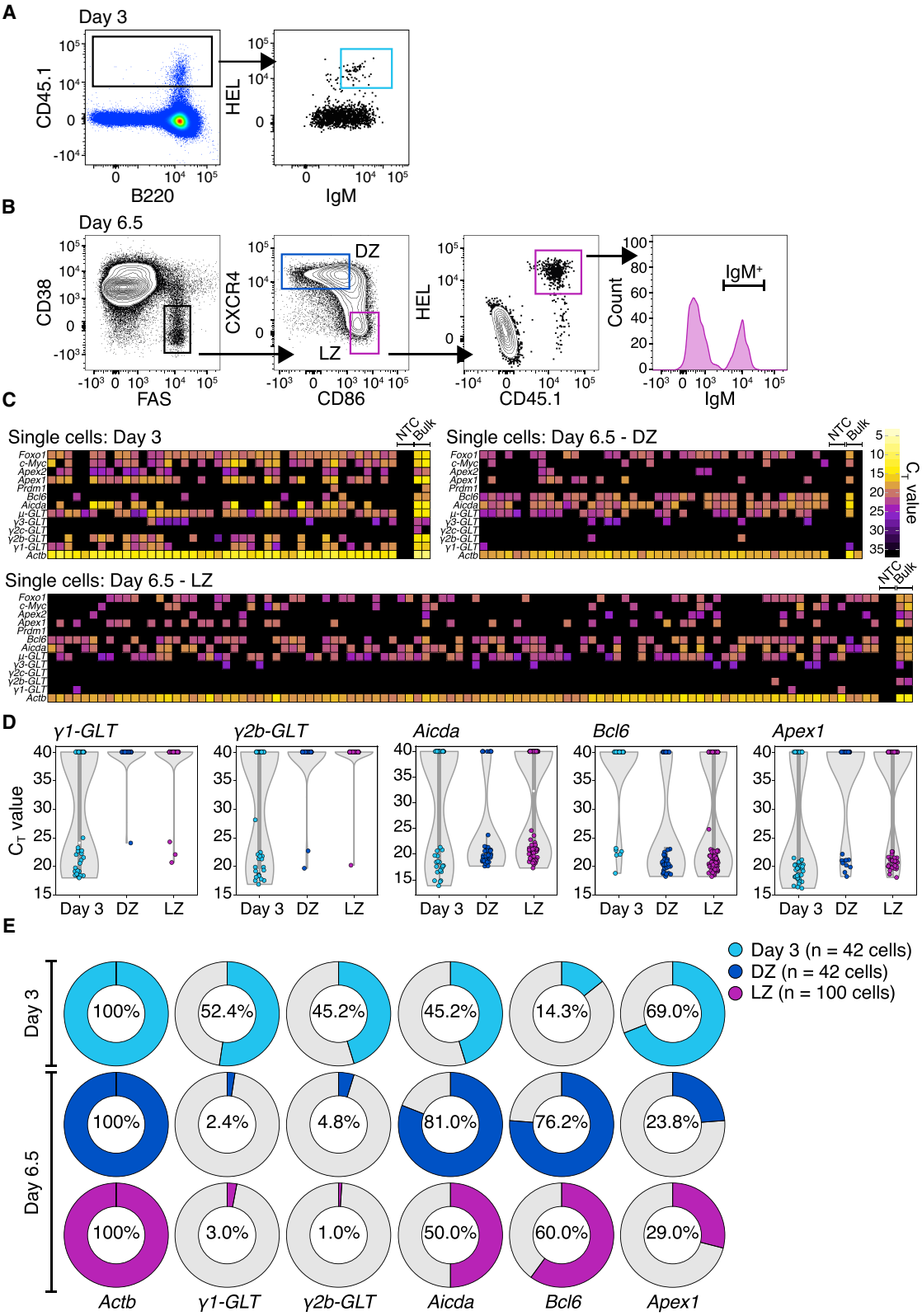

(legend on next page)

primary follicles that had yet not formed GCs. Within the following 48 h, GFP$^+$ cells were seen filling both GCs and extrafollicular foci. Thus, similar to the SW$_{HEL}$ B cell response, class switching is induced outside the follicles 24 h prior to GC formation.

Single-Cell Profiling of DZ and LZ B Cells Reveals that GLTs are Greatly Diminished within GCs

To ensure we were not underestimating GLT production in light-zone (LZ) cells (centrocytes), thought to be the B cell subset in which GLT is activated (Liu et al., 1996), we performed single-cell qPCR studies (Figures 3A–3E). Single day 3 IgM$^+$ Sw$_{HEL}$ activated B cells and day 6.5 IgM$^+$ SW$_{HEL}$ GC B cells (Brink et al., 2015), subdivided into LZ and dark zone (DZ) cells according to CXCR4 and CD86 expression (Figures 3A, 3B, S3A, and S3B), were flow-cytometry purified. Compared to 52% of day 3 activated B cells expressing *γ1-GLT*, less than 3% of day 6.5 DZ or LZ B cells expressed this transcript (Figures 3C–3E). Similar results were observed for *γ2b-GLT*, with 45% of day 3 B cells positive but only 4.8% and 1% of DZ and LZ B cells, respectively, expressing this GLT (Figures 3C–3E). Of note, 38% of GLT-positive B cells expressed more than one GLT.

It has been suggested that CSR requires FOXO1 and c-MYC transcription factor coexpression (Sander et al., 2015). Consistent with this, ~70% of day 3 B cells were *Foxo1* and *c-Myc* double positive, and ~80% of these double-positive cells expressed GLTs (Figures S3C and S3D). By contrast, despite 41% of LZ cells expressing *Foxo1* and 9% coexpressing *Foxo1* and *c-Myc* (Figures 3C, and S3C, and S3D), none of the *Foxo1* and *c-Myc* double-positive LZ cells expressed GLTs (Figure S3D). This was also true for DZ B cells, with no double-positive cells expressing GLTs (Figures S3C and S3D). These results support the notion that GLT production leading to activation of CSR is not a feature of mature GCs.

GLTs Remain Low in Long-Lived GCs

We next sought to investigate responses to a different antigen and adjuvant and exclude the possibility that short-lived GCs, such as those induced by SRBC, may not be favorable to ongoing switching. For this, we transferred 4-hydroxy-3-nitrophenyl acetyl (NP)-reactive B1-8^{hi} tdTomato$^+$ (tdT$^+$) cells together with NP conjugated to chicken gamma globulin (CGG) (Shih et al., 2002) into C57BL/6 mice primed with CGG in complete Freund's adjuvant (CFA) 3 days earlier (Figures 4A, 4B, and S4A). This priming strategy makes the kinetics of the first few days comparable to those shown for SW$_{HEL}$ responses (Figure 1C) but with GCs persisting longer. Similar to the HEL$^{2\times}$-SRBC response, *γ1-GLT* peaked between days 2 and 2.5 (Figure 4C); at this time point, GLTs were found in cells with an intermediate phenotype (CD38^{int} FAS^{int}) between EFPB and GC B cells (Figures 4B and 4C). GLTs had declined considerably by day 6.5 (Figure 4C). At a later stage of this immune response (days 14–18; Figures 4D and 4E), GC B cells maintained low amounts of *γ1-GLT* (Figure 4F). Consistent with early induction of CSR, IgG expression in NP-binding B cells was first seen at day 2 (Figure 4G). IgG$^+$ GC B cells peaked and reached a plateau between days 4 and 8, remaining at constant numbers through day 18 (Figure 4G), a period in which GCs were sustained (Figure 4H). Thus, there was no evidence of reactivation or increased rates of Ig switching in the late stages of the GC response.

The product of the episomes looped out from the IgH locus after C$_H$ gene recombination, known as switch-circle transcripts, were assessed in all the adoptive transfer experiments performed. Despite efficient detection of switch-circle transcripts in B cells activated *in vitro* (Figures S4B and S4C), these byproducts of CSR could not be detected at any time point during the *in vivo* primary responses, either in pooled or single antigen-specific B cells (data not shown). This is likely to be due to the transient nature of these molecules and the low number of copies generated by a fraction of antigen-specific B cells. Of note, published studies measuring switch circle transcripts were conducted using *in vitro* culture systems or higher numbers of responding B cells such as those seen during reactivation of memory B cells (Kinoshita et al., 2001; Liu et al., 1996; McHeyzer-Williams et al., 2015; Wesemann et al., 2011).

Phylogenetic Analysis Reveals that CSR Occurs Prior to the Onset of SHM

In order to assess CSR in mice with a polyclonal repertoire without the need for adoptive transfers that might lead to underestimation of ongoing switching, we determined the timing of CSR in polyclonal GCs through phylogenetic analysis (Figures 5A–5C). For this, we performed *in situ* photoactivation of single GCs within lymph nodes from GFP-photoactivatable (GFP-PA) mice (Tas et al., 2016; Victora et al., 2010). This allows cells within the same GC to be fluorescently tagged and then flow-cytometry sorted as single-GC B cells. GFP-PA mice were immunized with CGG in alum, and photoactivation followed by flow-cytometry purification was performed 15 or 20 days later to allow multiple rounds of division and SHM within GCs. The SHM burden in the V region and the induction of recombination in the C$_H$ region was assessed by *Igh* mRNA sequencing in each cell. With this approach, clonal trees containing both switched and unswitched B cells can be used to establish the timing of CSR, where the CSR point can be inferred as the last common ancestor of the switched and unswitched cells. Thus, the number of somatic

Figure 3. Single-Cell Analysis of GLTs in Early-Activated and GC B Cells

(A and B) Flow-cytometry plots showing gating strategy to purify HEL-binding B cells after HEL$^{2\times}$-SRBC immunization. Donor-derived cells were single-cell purified as IgM$^+$HEL$^+$ B blasts (day 3) (A) and IgM$^+$HEL$^+$ GC B cells (day 6.5) (B). GC B cells were subdivided as either DZ or LZ cells based on CXCR4 and CD86 expression as shown.

(C) Heatmap showing single-cell qPCR expression profile of selected targets in B blasts and DZ and LZ SW$_{HEL}$ B cells purified as described in (A) and (B).

(D) Quantification of raw C$_T$ values for *γ1-GLT*, *γ2b-GLT*, *Aicda*, *Bcl6*, and *Apex1* obtained in (C). Violin plots depict data distribution; each dot represents an individual cell.

(E) Pie charts showing quantification of target genes as shown in (D). Numbers indicate the percentage of cells expressing the indicated target.

The limit of detection for analysis was set to 40 cycles; cells with a C$_T$ value <40 were considered positive events. NTC, no template control; Bulk, bulk population control of 20 cells. Data are representative of two independent experiments. See also Figure S3.

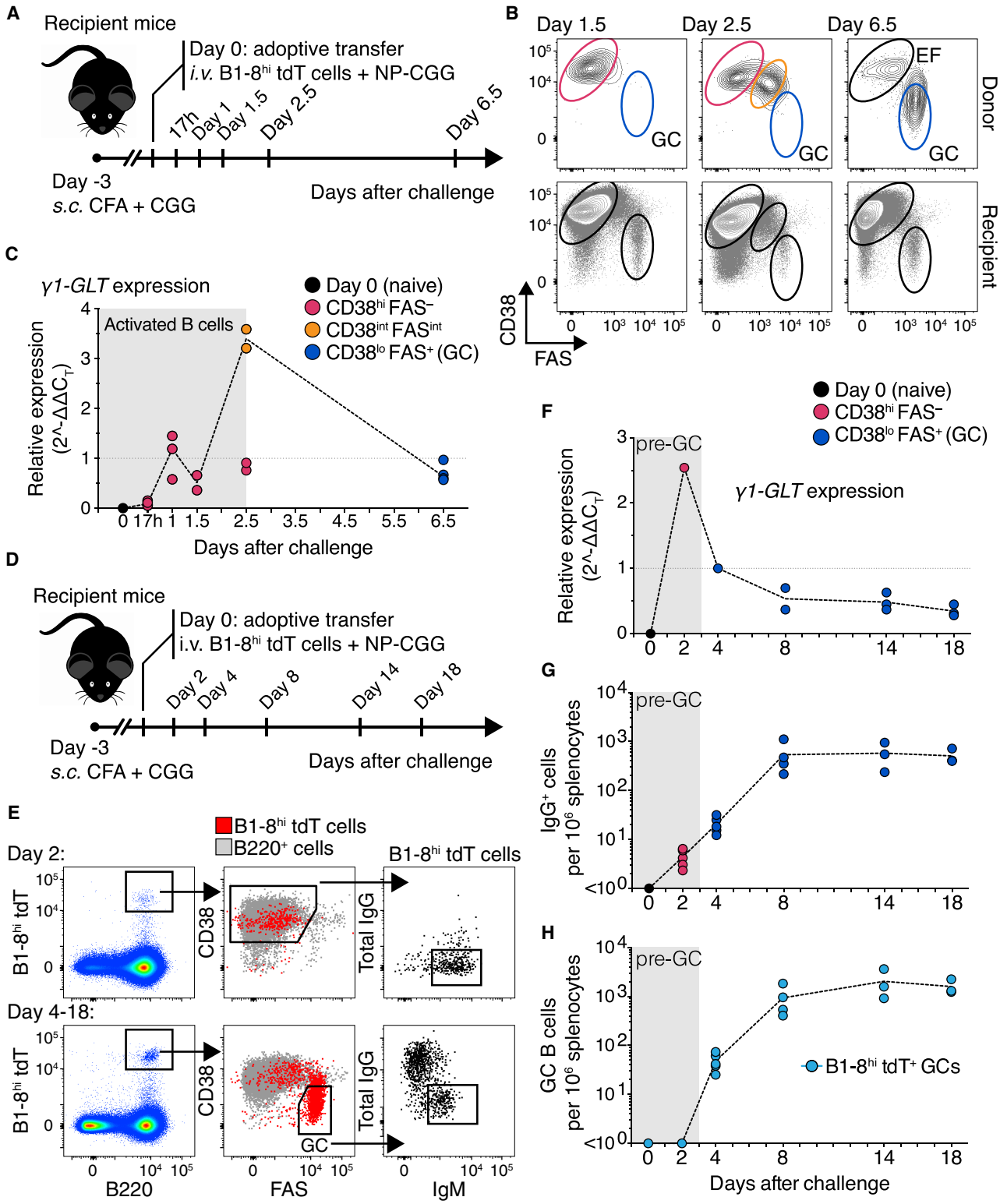

Figure 4. Expression of GLTs Remains Low in Late GC Responses

(A) Adoptive transfer protocol of B1-8^{hi} tdT^{+} B cells to investigate the early phases of the immune response to NP-CGG (see STAR Methods).

(B) Flow-cytometric plots showing gating strategy to identify B1-8^{hi} tdT^{+} B cells as shown in (A). Top panel shows representative plots of CD38 versus FAS for donor-derived B1-8^{hi} tdT^{+} B cells, and bottom panel shows the profile for recipient cells in the same mouse.

(C) qPCR gene-expression profile for *γ1-GLT* in purified donor-derived B1-8^{hi} tdT^{+} B cells as for (A) and (B). See (F) for details.

(legend continued on next page)

mutations at the inferred CSR point serves as a "molecular time stamp," which can be compared to the total SHM burden of cells present in the GC at the time of analysis: CSR points occurring in cells with zero mutations would indicate that CSR precedes SHM and therefore occurs prior to GC onset, whereas CSR points occurring in cells that have accumulated mutations would suggest that CSR is an ongoing process in GCs.

IgG1 is the most common isotype found in the CGG-alum response. To maximize the possibility of identifying IgM to IgG1 CSR events, we screened GCs for expanded IgM^+ and IgG^+ B cell clones, including in the analysis clones containing ≥ 4 IgM^+ cells (Figure S5A). This approach led to sequencing 13 clones, including all eight clones that contained both IgM and IgG cells (Figures 5A and 5B). Phylogenetic trees were displayed against the number of somatic mutations in each cell (x axis in Figure 5B), where the inferred CSR points are depicted as red filled triangles (Figure 5B). We found that several trees remained IgM^+, indicative of not having switched after entering the GC; these were attributed a CSR point of zero (red open triangles, Figure 5B). Whereas the overall mutation burden in GC B cells was substantial (Figure 5C; mean of 5 mutations per cell), most clones had switch points at zero mutations, with a few at one mutation, and only a single clone underwent switching at an inferred branch point bearing four mutations. Importantly, we found a number of highly expanded and diversified clones (e.g., the top two clones at days 15 and 20 in Figure 5B) for which CSR was either not detected or occurred in a common precursor with zero or one mutations (Figures 5B and 5C). Thus, substantial SHM can occur in the absence of detectable CSR. Of note, no sequential switching events were detected in GCs, with IgG1, IgG2b, and IgG3 always arising directly from IgM^+ cells (Figure 5B). Similar findings were obtained from analysis of clonal trees within GCs from Peyer's patches: there were no CSR events within GC regardless of whether the trees were enriched in IgM^+, IgA^+, or $IgG2b^+$ cells Figures S5B and S5C). These data support previous evidence that IgA switching predominantly occurs outside germinal centers (Reboldi et al., 2016). Mutational analysis of polyclonal GCs supports that CSR is restricted to the pre-GC or early GC periods and is uncommon after cells have accumulated several mutations in mature GCs.

In Silico Modeling of CSR Predicts Lack of Ongoing Switching in GCs

Prominent IgM^+ GC responses have been previously reported in responses to SRBC cells, although these are relatively short lived (Shinall et al., 2000). Our detection of IgM-dominated GCs late in the response argues against ongoing switching (Figure 5A, green-dominated columns). This prompted us to analyze *in silico* whether constant versus decaying CSR would differ in the distribution of isotype-dominated GCs (Meyer-Hermann, 2014, Binder and Meyer-Hermann, 2016; Meyer-Hermann et al., 2012). Analysis of the isotype diversity of *in silico* GCs revealed that with constant switching, the probability of finding IgM-dominated GCs was negligible (Figure 5D), even when combined with a preferential output of switched GC B cells (Figure 5E) (Martin and Goodnow, 2002). These results were generated with constant influx of IgM-dominated B cells until day 6 post immunization but still hold true with ongoing influx of IgM^+ B cells for longer time periods (Figures S6A and S6B) or with a higher antigen-uptake rate of IgM B cells (Figures S6C and S6D). Thus, with a constant switching probability, no tested isotype-specific differences allowed induction of both IgM- and IgG-dominated GCs in the same setting, as required by our experimental results. In contrast, with a decaying-switching probability using a decay constant derived from the dynamics of *γ1-GLT* expression (Figure 1E), a broad spectrum of IgM- or IgG-dominated GCs develops (Figure 5F). As we have seen IgM-dominated GCs (Figures 5A and 5B), this result supports a model with CSR limited to the first days of the GC reaction. Next, we shifted the time at which the decay starts from day 3.5 post immunization (GC onset) to day 19.5 in our *in silico* model, keeping the integrated switching probability unchanged (Figure 5G). The resulting isotype diversity of GC simulations dropped when CSR occurred later than days 6–7 post immunization (Figure 5G). This suggests that a determination of the isotype before the GC phase of intense B cell selection promotes diversification of the GC isotype dominance at later times, while an ongoing switching probability would homogenize the isotype distribution of GC output.

APE1 Endonuclease Is Downregulated in Germinal Center B Cells

Our data so far demonstrated that downregulation of GLT production is a potent mechanism to dampen CSR in GCs. We considered the possibility of additional mechanisms that might contribute to limit CSR within GCs operating downstream of GLT production. Once GLTs have been produced, CSR relies on activation of AID, UNG, and APE1 to target S regions (Guikema et al., 2007; Muramatsu et al., 2000; Rada et al., 2002). APE1 is required in a dose-dependent manner during CSR (Masani et al., 2013; Xu et al., 2014), whereas it is dispensable for SHM (Stavnezer et al., 2014). By contrast, SHM does not need APE1 but instead requires APE2 (Masani et al., 2013; Sabouri et al., 2009; Stavnezer et al., 2014). We compared RNA expression data of these enzymes in human naive versus GC B cells.

(D) Adoptive transfer protocol of B1-8^{hi} tdT^+ B cells to investigate the late phases of the immune response to NP-CGG. C57BL/6 mice were immunized as shown in (A).

(E) Flow-cytometric plots showing gating strategy to analyze surface expression of total IgG at day 2 (top panel) and days 4–18 (bottom panel) in splenocytes harvested from mice immunized as in (D).

(F) qPCR gene-expression profile for γ1-GLT in purified donor-derived B1-8^{hi} tdT^+ B cells as shown in (D). Duplex qPCR analyses were conducted using *Actb* as reference gene. Data are presented as a fold change compared to day 1.0 B cells (C) or day 4 GC B cells (F) using the $\Delta\Delta C_T$ method. Dots represent individual mice. Black dotted lines connect the group medians.

(G and H) Flow-cytometric quantification of total IgG in donor-derived B1-8^{hi} tdT^+ cells (G) and total numbers of B1-8^{hi} tdT^+ GC B cells (H) in the spleens of recipient mice identified as in (D). Number of mice used in each time point: n = 5 (day 2), n = 5 (day 4), n = 4 (day 8), n = 5 (day 14), and n = 5 (day 18). Total cell numbers were normalized to 1×10^6 splenocytes.

Data are representative of three independent experiments. See also Figure S4.

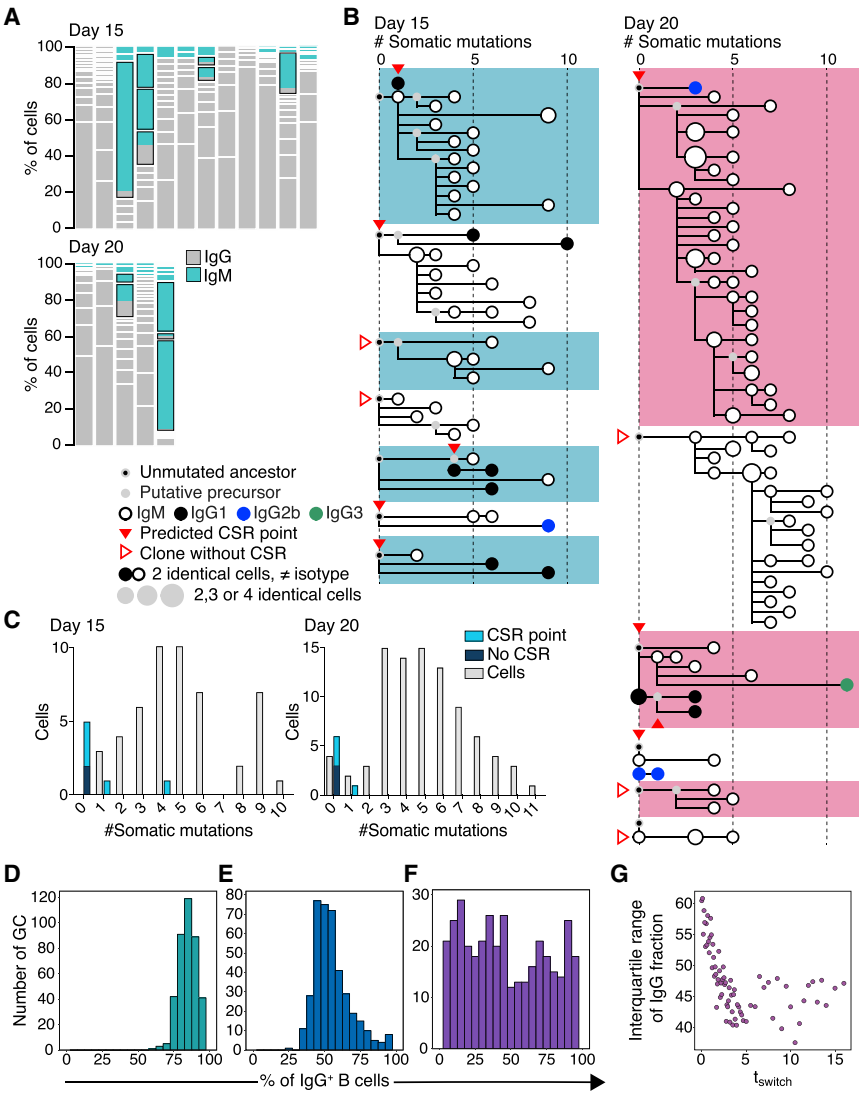

Figure 5. Lack of Ongoing Switching in IgM$^+$ B Cells from Established GCs and *In Silico* Modeling

(A) Schematic representation of the clonal and isotype composition of the GCs obtained from the popliteal lymph nodes (pLNs) of GFP-PA mice immunized 15 or 20 days earlier with CGG in alum. Each column represents a single GC, and the boxes in each column represent individual clones determined by phylogenetic analysis of single-cell mRNA V_H sequences. The size of each box has been scaled to reflect the number of cells in each clone. Grey represents IgG$^+$ B cells, and green represents IgM$^+$ B cells, as determined by *Igh* mRNA sequences. The boxes outlined in black indicate those selected for the somatic mutation analysis depicted in (B) based on mixed composition by both IgG$^+$ and IgM$^+$ cells and the presence of four or more IgM$^+$ cells (see STAR Methods).

(B) Charts showing clonal trees representing the phylogeny of V_H sequences within B cell clones (symbols according to the legend in the bottom panel).

(C) Summary of the data in (A) and (B) showing the SHM content of individual B cells at the time of the inferred switch event (filled red arrowheads). Clones containing only IgM$^+$ cells (empty red arrowheads) were pooled with those in which switching occurred at the level of the unmutated precursor (zero mutations). For each time point, five different mice in three independent experiments were included.

(D–F) Histograms showing distribution of IgG fractions at the end of affinity maturation *in silico* in (D) constant switching probability of p = 0.03 (D), constant switching probability combined with an increased probability of IgG$^+$ cells to leave the GC (E), and dynamic switching with an initial switching probability of p = 0.15 and a decaying switching probability of γ = 0.035 h^{-1} (F) (see Figure 1E). Each distribution shows the fraction of IgG$^+$ B cells at day 21 after the onset of the GC reaction.

(G) Effect of class-switch timing on the diversity of Ig isotypes in simulated GCs. t_{switch} (horizontal axis) denotes the time post GC onset (time post immunization minus 3.5 days) at which CSR is started with a decreasing probability. Each point corresponds to the interquartile range of the IgG fraction among B cells at the end of *in silico* GC reactions in 400 simulations.

See also Figures S5 and S6.

Expression of *AID*, *UNG*, and *APEX2* were all increased in GC B cells, whereas *APEX1* appeared downregulated (Figure 6A). These observations are consistent with a previous report in bulk mouse GC B cells (Stavnezer et al., 2014). We next asked whether APE1 downregulation is a feature of both LZ and DZ B cells (Figure 6B). Our data revealed a significant decline in APE1 protein in both DZ and LZ areas of human GCs (Figures 6B–6E). Thus, in addition to greatly diminished GLT induction in GC B cells, APE1 downregulation emerges as an additional backup mechanism to prevent CSR in GCs.

BCL6 Binds the Promoter Region of γ1-GLT and APE1

We next considered whether BCL6, the transcriptional repressor that determines the GC B cell fate, could contribute to the downregulation of GLTs, *Apex1* or both. BCL6 has been reported to bind to the ε-*GLT* promoter (Audzevich et al., 2013). We therefore tested whether this was also the case for the promoter of *γ1-GLT*. Bioinformatic analysis in the mouse promoter region of *γ1-GLT* revealed the presence of putative binding sites for BCL6 (Figures S6E–S6G). We used chromatin immunoprecipitation (ChIP)-qPCR to validate this observation using the Nojima coculture system to induce *in vitro*-derived GC (iGC) B cells (Kuraoka et al., 2016; Nojima et al., 2011). We found that indeed, BCL6 binds the promoter region of *γ1-GLT* (Figures S6H and S6I). Our analysis of published ChIP-on-chip data (Ci et al., 2009) revealed BCL6 was bound to the *APEX1* promoter regions, but not *APEX2* promoter regions, in human primary GC B cells (Figure 6F), as well as to the promoters of the well-established BCL6 targets, *TLR1* and *BCL6*. Thus, BCL6 may also act as key regulator of CSR by actively repressing the transcription of GLTs and APE1 expression in GC B cells.

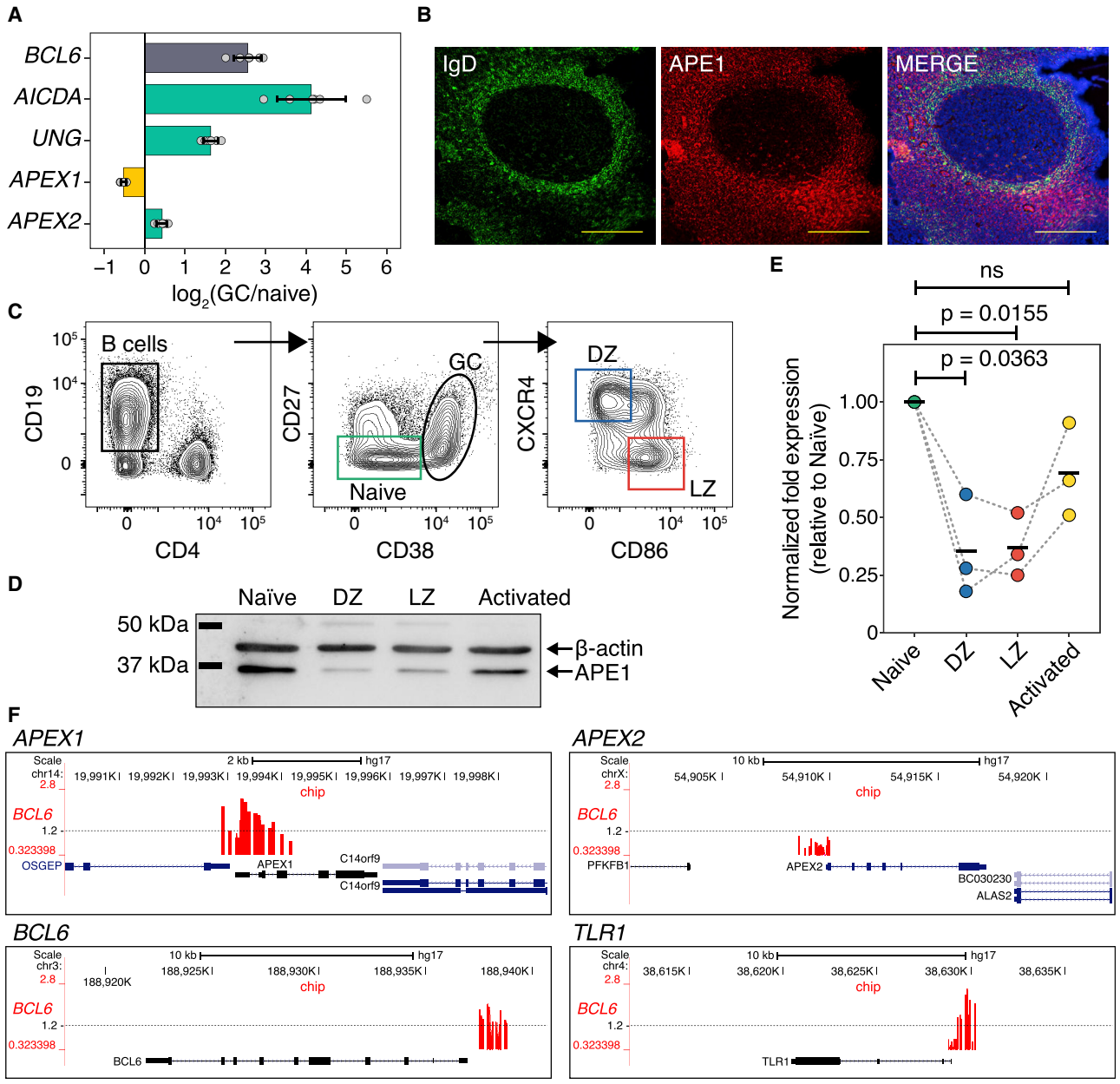

Figure 6. APE1 Is Downregulated in Human GC B Cells and Its Expression Is Modulated by BCL6

(A) Bar plot showing expression of human *BCL6*, *AICDA*, *UNG*, *APEX1*, and *APEX2* genes from purified tonsillar naive B cells and GC B cells by RNA-seq. Data are presented as the log2 fold change between reads per kilobase per million (RPKMs) of GC B cells relative to those on naive B cells. The bars represent means and error bars ± SD. Dots represent individual donors (n = 5).

(B) Immunofluorescence images of human tonsil samples showing APE1 (red), IgD (green), and DAPI (blue). Scale bars are 200 μm.

(C) Flow-cytometric plots showing the gating strategy to purify naive, DZ, and LZ B cells from human tonsils. Activated B cells correspond to naive B cells stimulated *in vitro* for 72 h with IL-21 and CD40L.

(D) Immunoblot of human APE1 protein in naive, DZ, LZ, and activated B cells. β-actin was used as a loading control.

(E) Quantification of APE1 protein by densitometry as for blot in (D). APE1 expression was normalized using β-actin. Data are presented as a fold change relative to naive B cells. Horizontal black bars represent means and dotted gray lines connect samples derived from the same tonsil donor. Numbers on top indicate the respective p value from two-tailed paired t test analysis; n = 3 donors.

(F) Regions where BCL6 binds to the promoter region of the genes encoding for APE1 (*APEX1*), APE2 (*APEX2*), BCL6, and TLR1 as determined by ChIP on chip (Ci et al., 2009).

See also Figure S6.

DISCUSSION

Here, we have shown that, unlike the prevailing idea that CSR is favored in GCs, this process largely occurs outside GCs. The association between CSR and GCs was first established when AID was discovered and shown to be expressed mainly in GCs and essential for both SHM and CSR (Muramatsu et al., 2000). Further studies mapped the cells expressing GLTs in humans to centrocytes on the basis of markers no longer used (Liu et al., 1996), since they identify a heterogenous population that also contains activated B cells (Högerkorp and Borrebaeck, 2006). Studies describing lack of CSR in mice lacking GCs further cemented the notion that CSR was a GC process; these mice also had defective T cell:B cell encounters needed for CSR.

We have provided several lines of evidence that collectively show that isotype switching is activated before GC formation and rapidly declines as B cells differentiate in EFPBs or GCs during a primary immune response against T cell-dependent (TD) antigens. CSR is initiated as early as day 1.5 following immunization and before GC formation via the production of GLTs. Analysis of GLT expression at the single-cell level in purified IgM^+ activated B cells and IgM^+ GC B cells provided evidence that GLTs were produced at very small amounts in mature GCs. Phylogenetic trees constructed from *Igh*-mRNA sequencing of photoactivated GC B cells demonstrated that CSR ceased soon after the onset of SHM. These trees also revealed the existence of IgM-dominated GCs, which are unlikely to occur under the assumption of ongoing switching. GLTs were first visualized at the T cell:B cell border prior to GC formation in a polyclonal B cell response using Cγ1-Cre:mT/mG mice, and a comparable proportion of class-switched B cells were found in the EF and follicular areas of the spleen, with no further enrichment within GCs. This was independent of the immunizing antigen, the longevity of the GC response, or the adjuvant used. Together, our work demonstrates early CSR with rapid decline in GCs, challenging the general belief that CSR is predominantly a GC process.

IgM^+ memory B cells are likely to be necessary to maintain a reservoir of antigen-experienced B cells (Reynaud et al., 2012) that can be rapidly engaged upon infection with either evolving or antigenically related pathogens (Bernasconi et al., 2002; Pape et al., 2011) but are not functionally committed to any particular effector process, which includes preserving their capacity to switch to any isotype. This, in turn, would result in a much broader spectrum of antigen-specific B cells, both in terms of BCR affinities and functional properties, filling the memory B cell compartment after each immunization. Our *in silico* modeling suggests that with constant CSR, the probability of IgM^+ GC B cells, and by extrapolation antigen-experienced IgM^+ memory B cells, is greatly diminished. By contrast, an early downregulation of switching increases isotype diversity. It is well known that humoral memory in humans can last for many years—even decades. IgM^+ memory B cells are considered more stable over time compared to their class-switched counterpart and thus represent a reservoir of lymphoid memory that can be induced at recall when the titers of primary protective antibodies have declined (Pape et al., 2011).

Lack of ongoing switching in GCs may be an important determinant of GC kinetics given the evidence that IgM and IgG tails have different influences on B cell behavior (Martin and Goodnow, 2002). It is possible that the larger GCs found in GCs of AID-deficient mice that cannot undergo CSR and are therefore IgM-dominated (Muramatsu et al., 2000) may reflect a greater permanence of IgM in GCs compared to their IgG counterparts. There is some evidence that switched and unswitched memory B cells have different transcriptional profiles (Seifert et al., 2015), suggesting important functional differences. Understanding what these differences are will also help explain further the biological significance of reducing CSR in GCs.

It is likely that low expression of AID, which is first detected on day 2.5, in conjunction with APE1 are sufficient for CSR; whereas high expression of AID and APE2 in GCs might be required for SHM. APE1 protein expression was reduced in GC B cells, including DZ and LZ B cells. These data were confirmed by RNA sequencing (RNA-seq) and in single-cell studies, where fewer GC B cells expressed *Apex1* mRNA compared to early-activated B cells. While AID is lowly expressed in recently activated B cells compared to GC B cells, CSR is considered very efficient in nature (Stavnezer et al., 2008): AID can attack anywhere within the S region, which can extend as long as 10–12 kb, resulting in a high likelihood of inducing the DNA breaks required for CSR. We therefore propose that CSR is induced early during B cell activation, and then it is silenced in GCs due to several mechanisms, including a reduction in GLT production and in APE1 protein. The latter is likely mediated by the transcriptional repressor BCL6, as suggested by BCL6 binding to the *Apex1* promoter.

Our data are compatible with the notion that naive B cells undergo CSR upon interacting with antigen and receiving T cell help prior to GC entry. We speculate that memory B cells may undergo CSR also upon interaction with T cells outside GCs, prior to differentiation into EFPBs or re-entry into a GC. Sequential class switching of memory B cells to downstream isotypes is well documented, at least in the context of IgE responses (He et al., 2015). CSR not only appears to be repressed in GCs; previous studies have suggested that CSR also ceases upon B cell differentiation into plasmablasts in a BLIMP1-mediated manner (Shaffer et al., 2002).

Besides being the core APE for CSR, APE1 is probably best known for its vital role in the base excision-repair (BER) pathway, an important arm of the DNA damage response that repairs with high-fidelity damaged bases (Fortini and Dogliotti, 2007; Krokan and Bjørås, 2013). Under normal circumstances, APE1 recruits several BER components to execute the repair of apurinic-apyrimidinic (AP) sites. Considering that APE1 is essential for cell survival and is ubiquitously expressed in all cells (Al-Safi et al., 2012; Fung and Demple, 2005; Xanthoudakis et al., 1996), the downregulation of APE1 in GC B cells is surprising although in line with published data (Stavnezer et al., 2014). APE1 downregulation may explain how DNA lesions introduced during SHM are spared from correct repair by the error-free BER machinery (Stavnezer et al., 2014). Indeed, the accurate repair of deoxyuridine (dU) residues generated by AID and UNG would antagonize the acquisition of somatic mutations in the IgV region needed for correct affinity maturation. This idea is further supported by the findings that DNA Polβ is not downregulated in GC B cells (Schrader et al., 2009). Complete abrogation of the BER pathway would

be risky in cases where off-target mutations arising outside the Ig locus demand faithful repair.

Programmed DNA damage during SHM and CSR is a tightly regulated event, yet off-target activity of AID causing double-strand DNA breaks outside the IgV and S regions has also been reported and contributes to genomic instability (Liu and Schatz, 2009). Up to 95% of all lymphoid cancers are believed to have a B cell origin as a consequence of AID-dependent gene translocations and fusions or mutations affecting *cis*-regulatory elements (Nussenzweig and Nussenzweig, 2010). CSR itself is an important contributor to DNA lesions, including aberrant gene translocations. Restricting CSR from taking place in GC B cells would help to reduce the likelihood of pathogenic double-strand breaks. Another potential advantage of limiting CSR in the GC comes from the observations of autoimmunity-inducing gene translocations or insertions occurring in the IgH locus during CSR (Nussenzweig and Nussenzweig, 2010; Tan et al., 2016): these occurrences would make this recombination process particularly risky in GCs, where not only are cells intensely proliferating, but also their output is destined to become long-lived memory B cells or plasma cells.

STAR★METHODS

Detailed methods are provided in the online version of this paper and include the following:

- KEY RESOURCES TABLE
- LEAD CONTACT AND MATERIALS AVAILABILITY
- EXPERIMENTAL MODEL AND SUBJECT DETAILS
  - Animals
  - Human samples
- METHOD DETAILS
  - SW_{HEL} B cell adoptive transfers
  - B1-8^{hi} tdTomato (tdT) B cell adoptive transfers
  - Flow cytometry analyses and FACS sorting
  - Immunofluorescence
  - *In vitro* B cell cultures
  - Immunoblot
  - qPCR analysis
  - One step qPCR analysis
  - Single cell qPCR
  - GC B cell clonal trees from GFP-photoactivatable (GFP-PA)-transgenic mice
  - Using AID-Cre-Confetti mice to track Peyer's Patch GCs
  - Nojima cell co-cultures
  - Chromatin immunoprecipitation (ChIP)-qPCR
  - Bioinformatic analysis of ChIP-on-chip datasets and prediction of BCL6-binding sites in GLTs
- QUANTIFICATION AND STATISTICAL ANALYSIS
  - Mathematical modeling
- DATA AND CODE AVAILABILITY

SUPPLEMENTAL INFORMATION

Supplemental Information can be found online at https://doi.org/10.1016/j.immuni.2019.07.001.

ACKNOWLEDGMENTS

The authors thank R. Brink for providing $HEL^{2\times}$ and $HEL^{3\times}$ protein and Sw_{HEL} mice; M. Nussenzweig for providing B1-8^{hi} tdTomato mice, S. Casola for providing Cγ1Cre:mT/mG mice, A. Prins for preparing histological samples, C. Gillespie for microscopy analysis, E. Bartlett for reviewing the manuscript, A. Wilson and A.-M. Hatch for assistance with obtaining tonsil samples and clinical data, the Australian Cancer Research Foundation (ACRF) Biomolecular Resource Facility (BRF) and the Australian Phenomics Facility (APF) for their technical support, the Imaging and Cytometry Facility at The John Curtin School of Medical Research—especially M. Devoy—for FACS sorting, W. Shi for analysis of RNA-seq data, and D. Kitamura and G. Kelsoe for kindly providing Nojima cells. C.G.V. is supported by fellowship, project, and program grants from the Australian National Health and Medical Research Council (APP1117812 and APP1113577). The Human Frontier Science Program (RGP0033/2015) supports M.M.-H., G.D.V., and C.G.V. G.D.V. is funded by NIH/NIAID grants R01AI119006 and R01AI139117.

AUTHOR CONTRIBUTIONS

J.A.R. conducted most of the experiments, figure editing, and data analysis. P.G.-F., P.F.C., J.E., Q.S., and J.C. helped with the experiments and human sample processing and provided intellectual input. H.V. provided intellectual input and expertise in the analysis and acquisition of flow cytometry data. L.M.C. provided help with the analysis of RNA-seq data. K.-M.T. provided intellectual input, helped in the design of single-cell studies, and together with Y.Z., performed the Cγ1-Cre:mT/mG mouse experiments. L.M., C.N., A.S., and G.D.V. performed the experiments using the GFP-PA and the AID-Cre-Confetti mouse models, generated clonal trees, provided intellectual input, and contributed to data analysis. S.C.B., P.A.R., and M.M.-H. provided intellectual input and performed the *in silico* modeling. C.R.N., J.A.R., and J.M.P. conducted the single-cell qPCR studies. J.A.R. and C.G.V. wrote the manuscript. C.G.V. was the main supervisor of this project. All authors reviewed the manuscript.

DECLARATION OF INTERESTS

The authors declare no competing interests.

Received: December 18, 2018
Revised: April 26, 2019
Accepted: July 9, 2019
Published: July 30, 2019

REFERENCES

Al-Safi, R.I., Odde, S., Shabaik, Y., and Neamati, N. (2012). Small-molecule inhibitors of APE1 DNA repair function: an overview. Curr. Mol. Pharmacol. *5*, 14–35.

Audzevich, T., Pearce, G., Breucha, M., Günal, G., and Jessberger, R. (2013). Control of the STAT6-BCL6 antagonism by SWAP-70 determines IgE production. J. Immunol. *190*, 4946–4955.

Bernasconi, N.L., Traggiai, E., and Lanzavecchia, A. (2002). Maintenance of serological memory by polyclonal activation of human memory B cells. Science *298*, 2199–2202.

Binder, S.C., and Meyer-Hermann, M. (2016). Implications of Intravital Imaging of Murine Germinal Centers on the Control of B Cell Selection and Division. Front. Immunol. *7*, 593.

Brink, R., Paus, D., Bourne, K., Hermes, J.R., Gardam, S., Phan, T.G., and Chan, T.D. (2015). The SW(HEL) system for high-resolution analysis of in vivo antigen-specific T-dependent B cell responses. Methods Mol. Biol. *1291*, 103–123.

Casola, S., Cattoretti, G., Uyttersprot, N., Koralov, S.B., Seagal, J., Hao, Z., Waisman, A., Egert, A., Ghitza, D., and Rajewsky, K. (2006). Tracking germinal center B cells expressing germ-line immunoglobulin gamma1 transcripts by conditional gene targeting. Proc. Natl. Acad. Sci. USA *103*, 7396–7401.

Cerutti, A. (2008). The regulation of IgA class switching. Nat. Rev. Immunol. *8*, 421–434.

Chan, T.D., Gatto, D., Wood, K., Camidge, T., Basten, A., and Brink, R. (2009). Antigen affinity controls rapid T-dependent antibody production by driving the expansion rather than the differentiation or extrafollicular migration of early plasmablasts. J. Immunol. *183*, 3139–3149.

Ci, W., Polo, J.M., Cerchietti, L., Shaknovich, R., Wang, L., Yang, S.N., Ye, K., Farinha, P., Horsman, D.E., Gascoyne, R.D., et al. (2009). The BCL6 transcriptional program features repression of multiple oncogenes in primary B cells and is deregulated in DLBCL. Blood *113*, 5536–5548.

Cogné, M., and Birshtein, B.K. (2004). CHAPTER 19 - Regulation of Class Switch Recombination A2 - Honjo, Tasuku. In Molecular Biology of B Cells, F.W. Alt and M.S. Neuberger, eds. (Burlington: Academic Press), pp. 289–305.

DeWitt, W.S., 3rd, Mesin, L., Victora, G.D., Minin, V.N., and Matsen, F.A., 4th (2018). Using Genotype Abundance to Improve Phylogenetic Inference. Mol. Biol. Evol. *35*, 1253–1265.

Fagarasan, S., Kinoshita, K., Muramatsu, M., Ikuta, K., and Honjo, T. (2001). In situ class switching and differentiation to IgA-producing cells in the gut lamina propria. Nature *413*, 639–643.

Fortini, P., and Dogliotti, E. (2007). Base damage and single-strand break repair: mechanisms and functional significance of short- and long-patch repair subpathways. DNA Repair (Amst.) *6*, 398–409.

Fung, H., and Demple, B. (2005). A vital role for Ape1/Ref1 protein in repairing spontaneous DNA damage in human cells. Mol. Cell *17*, 463–470.

Gitlin, A.D., Shulman, Z., and Nussenzweig, M.C. (2014). Clonal selection in the germinal centre by regulated proliferation and hypermutation. Nature *509*, 637–640.

Guikema, J.E., Linehan, E.K., Tsuchimoto, D., Nakabeppu, Y., Strauss, P.R., Stavnezer, J., and Schrader, C.E. (2007). APE1- and APE2-dependent DNA breaks in immunoglobulin class switch recombination. J. Exp. Med. *204*, 3017–3026.

He, J.S., Narayanan, S., Subramaniam, S., Ho, W.Q., Lafaille, J.J., and Curotto de Lafaille, M.A. (2015). Biology of IgE production: IgE cell differentiation and the memory of IgE responses. Curr. Top. Microbiol. Immunol. *388*, 1–19.

Högerkorp, C.M., and Borrebaeck, C.A. (2006). The human CD77- B cell population represents a heterogeneous subset of cells comprising centroblasts, centrocytes, and plasmablasts, prompting phenotypical revision. J. Immunol. *177*, 4341–4349.

Jacob, J., Kassir, R., and Kelsoe, G. (1991). In situ studies of the primary immune response to (4-hydroxy-3-nitrophenyl)acetyl. I. The architecture and dynamics of responding cell populations. J. Exp. Med. *173*, 1165–1175.

Kagey, M.H., Newman, J.J., Bilodeau, S., Zhan, Y., Orlando, D.A., van Berkum, N.L., Ebmeier, C.C., Goossens, J., Rahl, P.B., Levine, S.S., et al. (2010). Mediator and cohesin connect gene expression and chromatin architecture. Nature *467*, 430–435.

Kawabe, T., Naka, T., Yoshida, K., Tanaka, T., Fujiwara, H., Suematsu, S., Yoshida, N., Kishimoto, T., and Kikutani, H. (1994). The immune responses in CD40-deficient mice: impaired immunoglobulin class switching and germinal center formation. Immunity *1*, 167–178.

Khan, A., Fornes, O., Stigliani, A., Gheorghe, M., Castro-Mondragon, J.A., van der Lee, R., Bessy, A., Chèneby, J., Kulkarni, S.R., Tan, G., et al. (2018). JASPAR 2018: update of the open-access database of transcription factor binding profiles and its web framework. Nucleic Acids Res. *46* (D1), D1284.

Kinoshita, K., Harigai, M., Fagarasan, S., Muramatsu, M., and Honjo, T. (2001). A hallmark of active class switch recombination: transcripts directed by I promoters on looped-out circular DNAs. Proc. Natl. Acad. Sci. USA *98*, 12620–12623.

Klein, U., and Dalla-Favera, R. (2008). Germinal centres: role in B-cell physiology and malignancy. Nat. Rev. Immunol. *8*, 22–33.

Krokan, H.E., and Bjørås, M. (2013). Base excision repair. Cold Spring Harb. Perspect. Biol. *5*, a012583.

Kuraoka, M., Schmidt, A.G., Nojima, T., Feng, F., Watanabe, A., Kitamura, D., Harrison, S.C., Kepler, T.B., and Kelsoe, G. (2016). Complex Antigens Drive Permissive Clonal Selection in Germinal Centers. Immunity *44*, 542–552.

Lefranc, M.P., Giudicelli, V., Ginestoux, C., Jabado-Michaloud, J., Folch, G., Bellahcene, F., Wu, Y., Gemrot, E., Brochet, X., Lane, J., et al. (2009). IMGT, the international ImMunoGeneTics information system. Nucleic Acids Res. *37*, D1006–D1012.

Liu, M., and Schatz, D.G. (2009). Balancing AID and DNA repair during somatic hypermutation. Trends Immunol. *30*, 173–181.

Liu, Y.J., Malisan, F., de Bouteiller, O., Guret, C., Lebecque, S., Banchereau, J., Mills, F.C., Max, E.E., and Martinez-Valdez, H. (1996). Within germinal centers, isotype switching of immunoglobulin genes occurs after the onset of somatic mutation. Immunity *4*, 241–250.

Lorenz, M., Jung, S., and Radbruch, A. (1995). Switch transcripts in immunoglobulin class switching. Science *267*, 1825–1828.

Marshall, J.L., Zhang, Y., Pallan, L., Hsu, M.C., Khan, M., Cunningham, A.F., MacLennan, I.C., and Toellner, K.M. (2011). Early B blasts acquire a capacity for Ig class switch recombination that is lost as they become plasmablasts. Eur. J. Immunol. *41*, 3506–3512.

Martin, S.W., and Goodnow, C.C. (2002). Burst-enhancing role of the IgG membrane tail as a molecular determinant of memory. Nat. Immunol. *3*, 182–188.

Masani, S., Han, L., and Yu, K. (2013). Apurinic/apyrimidinic endonuclease 1 is the essential nuclease during immunoglobulin class switch recombination. Mol. Cell. Biol. *33*, 1468–1473.

McHeyzer-Williams, L.J., Milpied, P.J., Okitsu, S.L., and McHeyzer-Williams, M.G. (2015). Class-switched memory B cells remodel BCRs within secondary germinal centers. Nat. Immunol. *16*, 296–305.

Meyer-Hermann, M. (2014). Overcoming the dichotomy of quantity and quality in antibody responses. J. Immunol. *193*, 5414–5419.

Meyer-Hermann, M., Mohr, E., Pelletier, N., Zhang, Y., Victora, G.D., and Toellner, K.M. (2012). A theory of germinal center B cell selection, division, and exit. Cell Rep. *2*, 162–174.

Muramatsu, M., Kinoshita, K., Fagarasan, S., Yamada, S., Shinkai, Y., and Honjo, T. (2000). Class switch recombination and hypermutation require activation-induced cytidine deaminase (AID), a potential RNA editing enzyme. Cell *102*, 553–563.

Muzumdar, M.D., Tasic, B., Miyamichi, K., Li, L., and Luo, L. (2007). A global double-fluorescent Cre reporter mouse. Genesis *45*, 593–605.

Nefzger, C.M., Jardé, T., Rossello, F.J., Horvay, K., Knaupp, A.S., Powell, D.R., Chen, J., Abud, H.E., and Polo, J.M. (2016). A Versatile Strategy for Isolating a Highly Enriched Population of Intestinal Stem Cells. Stem Cell Reports *6*, 321–329.

Nojima, T., Haniuda, K., Moutai, T., Matsudaira, M., Mizokawa, S., Shiratori, I., Azuma, T., and Kitamura, D. (2011). In-vitro derived germinal centre B cells differentially generate memory B or plasma cells in vivo. Nat. Commun. *2*, 465.

Nussenzweig, A., and Nussenzweig, M.C. (2010). Origin of chromosomal translocations in lymphoid cancer. Cell *141*, 27–38.

Papa, I., Saliba, D., Ponzoni, M., Bustamante, S., Canete, P.F., Gonzalez-Figueroa, P., McNamara, H.A., Valvo, S., Grimbaldeston, M., Sweet, R.A., et al. (2017). T_{FH}-derived dopamine accelerates productive synapses in germinal centres. Nature *547*, 318–323.

Pape, K.A., Kouskoff, V., Nemazee, D., Tang, H.L., Cyster, J.G., Tze, L.E., Hippen, K.L., Behrens, T.W., and Jenkins, M.K. (2003). Visualization of the genesis and fate of isotype-switched B cells during a primary immune response. J. Exp. Med. *197*, 1677–1687.

Pape, K.A., Taylor, J.J., Maul, R.W., Gearhart, P.J., and Jenkins, M.K. (2011). Different B cell populations mediate early and late memory during an endogenous immune response. Science *331*, 1203–1207.

Paus, D., Phan, T.G., Chan, T.D., Gardam, S., Basten, A., and Brink, R. (2006). Antigen recognition strength regulates the choice between extrafollicular plasma cell and germinal center B cell differentiation. J. Exp. Med. *203*, 1081–1091.

Phan, T.G., Amesbury, M., Gardam, S., Crosbie, J., Hasbold, J., Hodgkin, P.D., Basten, A., and Brink, R. (2003). B cell receptor-independent stimuli trigger immunoglobulin (Ig) class switch recombination and production of IgG autoantibodies by anergic self-reactive B cells. J. Exp. Med. *197*, 845–860.

Phan, T.G., Gardam, S., Basten, A., and Brink, R. (2005). Altered migration, recruitment, and somatic hypermutation in the early response of marginal zone B cells to T cell-dependent antigen. J. Immunol. *174*, 4567–4578.

Rada, C., Williams, G.T., Nilsen, H., Barnes, D.E., Lindahl, T., and Neuberger, M.S. (2002). Immunoglobulin isotype switching is inhibited and somatic hypermutation perturbed in UNG-deficient mice. Curr. Biol. *12*, 1748–1755.

Reboldi, A., Arnon, T.I., Rodda, L.B., Atakilit, A., Sheppard, D., and Cyster, J.G. (2016). IgA production requires B cell interaction with subepithelial dendritic cells in Peyer's patches. Science *352*, aaf4822.

Retter, I., Althaus, H.H., Münch, R., and Müller, W. (2005). VBASE2, an integrative V gene database. Nucleic Acids Res. *33*, D671–D674.

Reynaud, C.A., Descatoire, M., Dogan, I., Huetz, F., Weller, S., and Weill, J.C. (2012). IgM memory B cells: a mouse/human paradox. Cell. Mol. Life Sci. *69*, 1625–1634.

Sabouri, Z., Okazaki, I.M., Shinkura, R., Begum, N., Nagaoka, H., Tsuchimoto, D., Nakabeppu, Y., and Honjo, T. (2009). Apex2 is required for efficient somatic hypermutation but not for class switch recombination of immunoglobulin genes. Int. Immunol. *21*, 947–955.

Sander, S., Chu, V.T., Yasuda, T., Franklin, A., Graf, R., Calado, D.P., Li, S., Imami, K., Selbach, M., Di Virgilio, M., et al. (2015). PI3 Kinase and FOXO1 Transcription Factor Activity Differentially Control B Cells in the Germinal Center Light and Dark Zones. Immunity *43*, 1075–1086.

Schrader, C.E., Guikema, J.E., Wu, X., and Stavnezer, J. (2009). The roles of APE1, APE2, DNA polymerase beta and mismatch repair in creating S region DNA breaks during antibody class switch. Philos. Trans. R. Soc. Lond. B Biol. Sci. *364*, 645–652.

Seifert, M., Przekopowitz, M., Taudien, S., Lollies, A., Ronge, V., Drees, B., Lindemann, M., Hillen, U., Engler, H., Singer, B.B., and Küppers, R. (2015). Functional capacities of human IgM memory B cells in early inflammatory responses and secondary germinal center reactions. Proc. Natl. Acad. Sci. USA *112*, E546–E555.

Shaffer, A.L., Lin, K.I., Kuo, T.C., Yu, X., Hurt, E.M., Rosenwald, A., Giltnane, J.M., Yang, L., Zhao, H., Calame, K., and Staudt, L.M. (2002). Blimp-1 orchestrates plasma cell differentiation by extinguishing the mature B cell gene expression program. Immunity *17*, 51–62.

Shih, T.A., Roederer, M., and Nussenzweig, M.C. (2002). Role of antigen receptor affinity in T cell-independent antibody responses in vivo. Nat. Immunol. *3*, 399–406.

Shinall, S.M., Gonzalez-Fernandez, M., Noelle, R.J., and Waldschmidt, T.J. (2000). Identification of murine germinal center B cell subsets defined by the expression of surface isotypes and differentiation antigens. J. Immunol. *164*, 5729–5738.

Shinkura, R., Matsuda, F., Sakiyama, T., Tsubata, T., Hiai, H., Paumen, M., Miyawaki, S., and Honjo, T. (1996). Defects of somatic hypermutation and class switching in alymphoplasia (aly) mutant mice. Int. Immunol. *8*, 1067–1075.

Snapper, C.M., and Mond, J.J. (1993). Towards a comprehensive view of immunoglobulin class switching. Immunol. Today *14*, 15–17.

Stavnezer, J. (1996). Immunoglobulin class switching. Curr. Opin. Immunol. *8*, 199–205.

Stavnezer, J., Guikema, J.E., and Schrader, C.E. (2008). Mechanism and regulation of class switch recombination. Annu. Rev. Immunol. *26*, 261–292.

Stavnezer, J., Linehan, E.K., Thompson, M.R., Habboub, G., Ucher, A.J., Kadungure, T., Tsuchimoto, D., Nakabeppu, Y., and Schrader, C.E. (2014). Differential expression of APE1 and APE2 in germinal centers promotes error-prone repair and A:T mutations during somatic hypermutation. Proc. Natl. Acad. Sci. USA *111*, 9217–9222.

Tan, J., Pieper, K., Piccoli, L., Abdi, A., Perez, M.F., Geiger, R., Tully, C.M., Jarrossay, D., Maina Ndungu, F., Wambua, J., et al. (2016). A LAIR1 insertion generates broadly reactive antibodies against malaria variant antigens. Nature *529*, 105–109.

Tangye, S.G., Avery, D.T., Deenick, E.K., and Hodgkin, P.D. (2003). Intrinsic differences in the proliferation of naive and memory human B cells as a mechanism for enhanced secondary immune responses. J. Immunol. *170*, 686–694.

Tas, J.M., Mesin, L., Pasqual, G., Targ, S., Jacobsen, J.T., Mano, Y.M., Chen, C.S., Weill, J.C., Reynaud, C.A., Browne, E.P., et al. (2016). Visualizing antibody affinity maturation in germinal centers. Science *351*, 1048–1054.

Toellner, K.M., Gulbranson-Judge, A., Taylor, D.R., Sze, D.M., and MacLennan, I.C. (1996). Immunoglobulin switch transcript production in vivo related to the site and time of antigen-specific B cell activation. J. Exp. Med. *183*, 2303–2312.

Victora, G.D., Schwickert, T.A., Fooksman, D.R., Kamphorst, A.O., Meyer-Hermann, M., Dustin, M.L., and Nussenzweig, M.C. (2010). Germinal center dynamics revealed by multiphoton microscopy with a photoactivatable fluorescent reporter. Cell *143*, 592–605.

Vinuesa, C.G., Sanz, I., and Cook, M.C. (2009). Dysregulation of germinal centres in autoimmune disease. Nat. Rev. Immunol. *9*, 845–857.

Wesemann, D.R., Magee, J.M., Boboila, C., Calado, D.P., Gallagher, M.P., Portuguese, A.J., Manis, J.P., Zhou, X., Recher, M., Rajewsky, K., et al. (2011). Immature B cells preferentially switch to IgE with increased direct Sμ to Sε recombination. J. Exp. Med. *208*, 2733–2746.

Xanthoudakis, S., Smeyne, R.J., Wallace, J.D., and Curran, T. (1996). The redox/DNA repair protein, Ref-1, is essential for early embryonic development in mice. Proc. Natl. Acad. Sci. USA *93*, 8919–8923.

Xu, J., Husain, A., Hu, W., Honjo, T., and Kobayashi, M. (2014). APE1 is dispensable for S-region cleavage but required for its repair in class switch recombination. Proc. Natl. Acad. Sci. USA *111*, 17242–17247.

STAR★METHODS

KEY RESOURCES TABLE

REAGENT or RESOURCE	SOURCE	IDENTIFIER
Antibodies		
APC/Cy7 anti-mouse/human CD45R/B220 Antibody (clone RA3-6B2)	BioLegend	Cat#103224; RRID: AB_313007
Alexa Fluor 647 anti-mouse Blimp-1 Antibody (clone 5E7)	BioLegend	Cat#150004; RRID: AB_2565618
Alexa Fluor 700 anti-mouse/human CD11b Antibody (clone M1/70)	BioLegend	Cat#101222; RRID: AB_493705
FITC Rat Anti-CD11b (clone M1/70)	BD Biosciences	Cat#553310; RRID: AB_394774
Purified Rat Anti-Mouse CD16/CD32 (mouse BD Fc Block, clone 2.4G2)	BD Biosciences	Cat#553142; RRID: AB_394657
Alexa Fluor 700 anti-mouse CD3 Antibody (clone 17A2)	BioLegend	Cat#100216; RRID: AB_493697
FITC Hamster Anti-Mouse CD3e (clone 145-2C11)	BD Biosciences	Cat#553062; RRID: AB_394595
CD38 Monoclonal Antibody (clone 90), Alexa Fluor 700	eBioscience	Cat#56-0381-82; RRID: AB_657740
BV421 Rat Anti-Mouse CD38 (clone 90/CD38)	BD Biosciences	Cat#562768; RRID: AB_2737781
PE anti-mouse CD38 Antibody (clone 90)	BioLegend	Cat#102707; RRID: AB_312928
Alexa Fluor 700 anti-mouse CD45.1 Antibody (clone A20)	BioLegend	Cat#110724; RRID: AB_493733
Pacific Blue anti-mouse CD45.1 Antibody (clone A20)	BioLegend	Cat#110722; RRID: AB_492866
BV421 Hamster Anti-Mouse CD95 (clone Jo2)	BD Biosciences	Cat#562633; RRID: AB_2737690
PE Hamster Anti-Mouse CD95 (clone Jo2)	BD Biosciences	Cat#554258; RRID: AB_395330
Biotin Rat Anti-Mouse CXCR5 (clone 2G8)	BD Biosciences	Cat#551960; RRID: AB_394301
IgD Monoclonal Antibody (clone 11-26c), FITC	eBioscience	Cat#11-5993-85; RRID: AB_465347
Biotin Rat Anti-Mouse IgG1 (clone A85-1)	BD Biosciences	Cat#553441; RRID: AB_394861
Biotin Rat Anti-Mouse IgG2a (clone R19-15)	BD Biosciences	Cat#550332; RRID: AB_393612
Biotin anti-mouse IgG2b Antibody (clone RMG2b-1)	BioLegend	Cat#406704; RRID: AB_315067
Biotin Mouse Anti-Mouse IgG2a[b] (clone 5.7)	BD Biosciences	Cat#553504; RRID: AB_394889
Biotin Rat Anti-Mouse IgG3 (clone R40-82)	BD Biosciences	Cat#553401; RRID: AB_394838
FITC Rat Anti-Mouse IgM (clone II/41)	BD Biosciences	Cat#553437; RRID: AB_394857
IgM Monoclonal Antibody (clone II/41), PE-Cy7	eBioscience	Cat#25-5790-82; RRID: AB_469655
PE-Cy7 Mouse Anti-Human CD19 (clone SJ25C1)	BD Biosciences	Cat#557835; RRID: AB_396893
FITC Mouse Anti-Human CD27 (clone M-T271)	BD Biosciences	Cat#555440; RRID: AB_395833
PE Mouse Anti-Human CD38 (clone HB7)	BD Biosciences	Cat#347687; RRID: AB_400341
APC-Cy7 Mouse Anti-Human CD4 (clone RPA-T4)	BD Biosciences	Cat#557871; RRID: AB_396913
BV421 Mouse Anti-Human CD86 (Clone 2331)	BD Biosciences	Cat#562432; RRID: AB_11153866
APC anti-human CD184 (CXCR4) Antibody (clone 12G5)	BioLegend	Cat#306510; RRID: AB_314616
Biotin anti-mouse CD3ε Antibody (clone 145-2C11)	BioLegend	Cat#100303; RRID: AB_312668
Purified Hamster Anti-Mouse CD3e (clone 145-2C11)	BD Biosciences	Cat#550275; RRID: AB_393572
Purified Rat Anti-Mouse IgD (clone 11-26c.2a)	BD Biosciences	Cat#553438; RRID: AB_394858
Ref-1 Antibody (anti-APE1, clone C-4)	Santa Cruz Biotechnology	Cat#sc-17774; RRID: AB_626685
Monoclonal anti-β-Actin antibody	Sigma	Cat#A5441; RRID: AB_476744
FITC Mouse Anti-Human IgD (clone IA6-2)	BD Biosciences	Cat#555778; RRID: AB_396113
anti-Bcl-6 antibody (clone N-3)	Santa Cruz Biotechnology	Cat#sc-858; RRID: AB_2063450
Biological Samples		
Human tonsills from concenting donors	The Canberra Hospital and Calvary John James Hospital (Canberra, ACT, Australia)	N/A

(*Continued on next page*)

Continued

REAGENT or RESOURCE	SOURCE	IDENTIFIER
Chemicals, Peptides, and Recombinant Proteins		
NP-CGG (ratio 30-39)	Biosearch Technologies	Cat#N-5055D-5
Complete Freund's adjuvant (CFA)	Sigma-Aldrich	Cat#F5881
Chicken gamma globulin (CGG)	Biosearch Techonolgies	Cat#C-1000-10
Streptavidin-APC	Thermo Fisher	Cat#S868
Streptavidin-BV605	BioLegend	Cat#405229
Streptavidin-Alexa Fluor 350	Thermo Fisher	Cat#S11249
Streptavidin-Alexa Fluor 405	Thermo Fisher	Cat#S32351
Human TruStain FcX (Fc Receptor Blocking Solution)	BioLegend	Cat#422302
FOXP3 Transcription Factor Staining Buffer Set	eBioscience	Cat#00-5523-00
Zombie aqua dye	BioLengend	Cat#423102
HEL^{2x} and $HEL3^{x}$ protein	Robert Brink	Paus et al., 2006
Trizol	Thermo Fisher	Cat#15596026
Recombinant Human IL-4	PeproTech	Cat#AF-200-04
Human IL-21	Miltenyi Biotec	Cat#130-094-563
Recombinant Murine IL-4	PeproTech	Cat#214-14
Recombinant Human sCD40 Ligand	PeproTech	Cat#310-02
RIPA buffer	Thermo Fisher	Cat#89901
Clarity Western ECL Substrate	Bio-Rad	Cat#1705061
Vectashield antifade mounting medium	Vector Laboratories	Cat#H-1000
Vectashield antifade mounting medium with DAPI	Vector Laboratories	Cat#H-1200
CellTrace Violet Cell Proliferation Kit	Thermo Fisher	Cat#C34571
7-Aminoactinomycin D (7-AAD)	Thermo Fisher	Cat#A1310
Complete, EDTA-free Protease Inhibitor Cocktail	Roche	Cat#11873580001
PhosStop (phosphatase inhibitor)	Roche	Cat#4906845001
Ficoll Paque Plus	GE Healthcare Life Sciences	Cat#17144003
Critical Commercial Assays		
PicoPure RNA Isolation Kit	Thermo Fisher	Cat#KIT0214
B Cell Isolation Kit, mouse	Miltenyi Biotech	Cat#130-090-862
Power SYBR Green PCR Master Mix	Thermo Fisher	Cat#4367659
QuantiTect Multiplex RT-PCR Kit	QIAGEN	Cat#204643
Single Cell-to-CT qRT-PCR Kit	Thermo Fisher	Cat#4458236
TaqMan Gene Expression Master Mix	Thermo Fisher	Cat#4369016
Deposited Data		
BCL6 ChIP-on-chip dataset	Ci et al., 2009	GEO: GSE15179
Experimental Models: Cell Lines		
Nojima cells	Daisuke Kitamura Garnett Kelsoe	Kuraoka et al., 2016; Nojima et al., 2011
Experimental Models: Organisms/Strains		
Mouse: B1-8^{hi} tdTomato	Michel Nussenzweig	Shih et al., 2002
Mouse: Cγ1Cre:mT/mG	Stefano Casola Kai-Michael Toellner	Casola et al., 2006
Mouse: GFP photoactivatable (GFP-PA)	Gabriel Victora	Victora et al., 2010
Mouse: AID-Cre-Confetti	Gabriel Victora	Tas et al., 2016
Mouse: C57BL/6NCrl	Charles River	Cat#027
Mouse: Sw_{HEL}	Robert Brink	Phan et al., 2003
Oligonucleotides		
Foxo1	Thermo Fisher	Cat#Mm00490672_m1
Prdm1	Thermo Fisher	Cat#Mm00476128_m1

(*Continued on next page*)

Continued

REAGENT or RESOURCE	SOURCE	IDENTIFIER
γ1-GLT: F: 5′-CGAGAAGCCTGAGGAATGTGT-3′ R: 5′-GGAGTTAGTTTGGGCAGCAGAT-3′ P: 5′-FAM-TGGTTCTCTCAACCTGTAGTCCATGCCA-3′	Biosearch Technologies	Marshall et al., 2011
*γ2b-GLT:*F: 5′-CGCACACCTACAGACAACCAG-3′ R: 5′-GTCACAGAGGAACCAGTTGTATC-3′ P: 5′-FAM-CCAGGGGGCCAGTGGATAGACTGAT-3′	Biosearch Technologies	Marshall et al., 2011
γ2c-GLT: F: 5′-GGACCACTAAAGCTGCTGACACAT-3′ R: 5′-AACCCTTGACCAGGCATCCT-3′P: 5′-FAM-AGCCCCATCGGTCTATCCACTGGC-3′	Biosearch Technologies	Marshall et al., 2011
γ3-GLT: F: 5′-GACCAAATTCGCTGAGTCATCA-3′R: 5′-ACCGAGGATCCAGATGTGTCA-3′P: 5′-FAM-CTGTCTATCCCTTGGTCCCTGGCTGC-3′	Biosearch Technologies	Marshall et al., 2011
μ-GLT: F: 5′-TCTGGACCTCTCCGAAACCA-3′ R: 5′-ATGGCCACCAGATTCTTATCAGA-3′ P: 5′-FAM-ATGTCTTCCCCCTCGTCTCCTGCG-3′	Biosearch Technologies	Marshall et al., 2011
Actb: F: 5′-CGTGAAAAGATGACCCAGATCA-3′R: 5′-TGGTACGACCAGAGGCATACAG-3′P: 5′-HEX-TCAACACCCCAGCCATGTACGTAGCC-3′	Biosearch Technologies	Marshall et al., 2011
Oligo(dT)$_{12-18}$ Primer	Thermo Fisher	Cat#18418012
Iγ1-P1: F: 5'-GCTCCACCTACCTTGTCTTTAT-3′ R: 5′-GAGATGGGTTCAGAGTGTCATAG-3′	Integrated DNA Technologies (IDT)	This paper
Iγ1-P2: F: 5′-CACTCTCACTCCAGGGTATAGA-3′ R: 5′-TGAGACCCAGAACACAGAATTAG-3′	Integrated DNA Technologies (IDT)	This paper
Iγ1-P3: F: 5′-CTCCCACAACCTGTACCTAAAT-3′ R: 5′-GGACATGGAAGTAGAGGATCAAA-3′	Integrated DNA Technologies (IDT)	This paper
Iγ1-P4: F: 5′-GTCAGGAAAGAGTGGGCATAA-3′ R: 5′-CTGGCTGTACTCCTGTTTCTC-3′	Integrated DNA Technologies (IDT)	This paper
Iγ1-TSS: F: 5′-GGGCAGGACCAAAACAGGAA-3′ R: 5′-TTTCCCTGCTGACCCCACTC-3′	Integrated DNA Technologies (IDT)	This paper
Aicda	Thermo Fisher	Cat#Mm01184115_m1
Apex1	Thermo Fisher	Cat#Mm01319526_g1
Actb	Thermo Fisher	Cat#Mm00607939_s1
Ubc	Thermo Fisher	Cat#Mm01198158_m1
Apex2	Thermo Fisher	Cat#Mm00518685_m1
Bcl6	Thermo Fisher	Cat#Mm00477633_m1
c-Myc	Thermo Fisher	Cat#Mm00487804_m1
Cd86	Thermo Fisher	Cat#Mm00444543_m1
Cxcr4	Thermo Fisher	Cat#Mm01292123_m1
Software and Algorithms		
In silico analysis of CSR (custom C++ code)	This paper	N/A
GraphPad Prism 7	GraphPad Software	RRID: SCR_002798
R version 3.3.3	The R Foundation for Statistical Computing	RRID: SCR_001905
Flowjo v10	FlowJo	RRID: SCR_008520
Adobe Photoshop	Adobe	RRID: SCR_014199
Adobe Illustrator	Adobe	RRID: SCR_010279

LEAD CONTACT AND MATERIALS AVAILABILITY

Further information and requests for resources and reagents should be directed to and will be fulfilled by the Lead Contact, Carola G. Vinuesa (carola.vinuesa@anu.edu.au).

EXPERIMENTAL MODEL AND SUBJECT DETAILS

Animals

C57BL/6, SW_{HEL} (Phan et al., 2003), B1-8^{hi} tdTomato (Shih et al., 2002), Cγ1Cre:mT/mG (Casola et al., 2006; Muzumdar et al., 2007), GFP-photoactivatable (GFP-PA) (Victora et al., 2010) and AID-Cre-Confetti (Tas et al., 2016) mice were bred and maintained in specific-pathogen-free conditions at The Australian National University (ANU), Canberra, Australia; The University of Birmingham, Birmingham UK; and The Rockefeller University, New York, USA. All experiments were performed according to the regulations approved by the local institution ethics committee, including The Australian National University's Animal and human Experimentation Ethics Committees.

Human samples

Human tonsils were obtained from consenting donors at The Canberra Hospital and Calvary John James Hospital (Canberra, ACT, Australia), following routine tonsillectomy. Tonsils were processed by mechanical disruption of the tissue and cells were isolated using Ficoll-Paque (#17144003, GE Healthcare Life Sciences) gradient centrifugation (Papa et al., 2017). All experiments with humans were approved by The Australian National University's Human Experimentation Ethics Committee and the University Hospitals Institutional Review Board.

METHOD DETAILS

SW_{HEL} B cell adoptive transfers

SW_{HEL} mice heterozygous for both light- and heavy-variable chain alleles of the anti-HEL BCR were sacrificed by cervical dislocation and splenocytes were collected. Single cell suspensions were obtained by mechanically disrupting the tissue through 70 μm nylon mesh filters (BD Biosciences) using complete RPMI 1640 media (Sigma-Aldrich). The exact frequency of SW_{HEL} B cells was determined by flow cytometry prior to adoptive transfer using HEL protein conjugated to Alexa Fluor 647 (A647). SW_{HEL} B cells ($CD45.1^+$) were resuspended in PBS 1x and adoptively transferred (intravenous injection; *i.v.*) into congenic C57BL/6 recipient mice ($CD45.2^+$) along with $2x10^8$ sheep red blood cells (SRBCs) conjugated to a mutated form of hen egg lysozyme (HEL^{2x} or HEL^{3x}) (Paus et al., 2006). For experiments analyzing the early stages of the immune response (days 1.0 - 2.5) $1.5x10^5$ HEL-binding cells were transferred; whereas for analysis of late phases (days 3 - 8.5) $3x10^4$ cells were given.

B1-8^{hi} tdTomato (tdT) B cell adoptive transfers

C57BL/6 recipient mice (8-10 weeks old) were pre-immunized by intraperitoneal (*i.p.*) injection of 100 μg of chicken gamma globulin (CGG; #C-1000-10, Biosearch Technologies) emulsified in complete Freund's adjuvant (CFA; #F5881, Sigma-Aldrich). Three days later, mice were intravenously transferred with B1-8^{hi} tdT^+ cells along with 50 μg of 4-hydroxy-3-nitrophenyl acetyl (NP) conjugated to CGG (ratio 30-39, #N-5055D-5, Biosearch Technologies). This mixture was delivered in 200 μL of PBS 1x. Single cell suspensions from B1-8^{hi} tdT^+ donor splenocytes were prepared in a similar fashion compared to SW_{HEL} B cell adoptive transfers. For investigation of early stages (17 h - day 1.5) of the immune response $1.8x10^5$ B1-8^{hi} tdT^+ cells were transferred. For late stages (days 2 - 18) recipient mice received $6x10^4$ B1-8^{hi} tdT^+ cells. The exact frequency of B1-8^{hi} tdT cells was determined by flow cytometry prior to transfer, as measured by binding of the hapten NP conjugated to APC.

Flow cytometry analyses and FACS sorting

Single cells suspensions were prepared from mouse spleens, lymph nodes and human tonsils as previously described (Papa et al., 2017; Tas et al., 2016). After processing, cell subsets were examined using flow cytometry using the following antibodies. For mouse tissues: B220-APCCy7 (#103224, BioLegend), BLIMP1 (#150004, BioLegend), CD11b-A700 (#101222, BioLegend), CD11b-FITC (#553310, BD Biosciences), CD16/32 (mouse Fc-block, #553142, BD Biosciences), CD3-A700 (#100216, BioLegend), CD3-biotin (#100303, BioLegend), CD3-FITC (#553062, BD Biosciences), CD38-A700 (#56-0381-82, eBioscience), CD38-BV421 (#562768, BD Biosciences), CD38-PE (#102707, BioLegend), CD45.1-PB (#110722, BioLegend), CD45.1-A700 (#110724, BioLegend), CD95-BV421 (#562633, BD Biosciences), CD95-PE (#554258, BD Biosciences), CXCR5-biotin (#551960, BD Biosciences), IgD-FITC (#11-5993-85, eBioscience), IgG1-biotin (#553441, BD Biosciences), IgG2a-biotin (#550332, BD Biosciences), IgG2b-biotin (#406704, BioLegend), IgG2c-biotin (#553504, BD Biosciences), IgG3-biotin (#553401, BD Biosciences), IgM-FITC (#553437, BD Biosciences), IgM-PECy7 (#25-5790-82, eBioscience), Streptavidin-APC (#S868, Thermo Fisher) and Streptavidin-BV605 (#405229, BioLegend). For human tonsils: CD19-PECy7 (#557835, BD Biosciences), CD27-FITC (#555440, BD Biosciences), CD38-PE (#347687, BD Biosciences), CD4-APCCy7 (#557871, BD Biosciences), CD86-A421 (#562432, BD Biosciences), CXCR4-APC (#306510, BioLegend) and Human TruStain FcX (Fc Receptor Blocking Solution, #422302, BioLegend). Antibody cocktails were prepared in flow cytometry buffer: PBS 1x (Sigma-Aldrich) containing 2% fetal bovine serum (FBS, GIBCO) and 2 mM EDTA (Sigma-Aldrich). For detection of HEL-binding cells, HEL protein (Sigma-Aldrich) was conjugated to A647 using a protein labeling conjugation kit (Thermo Fisher). Dead cells were excluded using either 7-Aminoactinomycin D (7-AAD, #A1310, Thermo Fisher) or Zombie aqua dye (#423102, BioLegend). Cells were stained with primary antibodies followed by secondary reagents for 30 min at

4°C in the dark. Intracellular stain was performed using the FOXP3 Transcription Factor Staining Buffer Set (#00-5523-00, eBioscience) according to the manufacturer's instructions. Samples were acquired on a LSRII or Fortessa cytometer (BD, Biosciences) and analyzed using FlowJo software v10 (FlowJo).

Immunofluorescence

Frozen tissue sections were fixed in cold acetone for 10-20 min. Donor-derived SW_{HEL} B cells were detected in the spleen of recipient mice as previously described (Paus et al., 2006). T cell areas were identified with anti-CD3-biotin antibody (#100303, BioLegend) followed by streptavidin conjugated to Alexa 350 (#S11249, Thermo Fisher). B cell follicles were visualized by staining with anti-IgD FITC (#11-5993-85, eBioscience). Cγ1-Cre:mT/mG spleen sections were stained with anti-CD3 (#550275, BD Biosciences) and anti-IgD (#553438, BD Biosciences) followed by biotin conjugated goat anti-hamster antibody (Jackson ImmunoResearch), streptavidin Alexa 405 (#S32351, Thermo Fisher) and donkey anti-rat Alexa-647 antibody (Jackson ImmunoResearch). For human samples, tonsil sections were blocked and permeabilized with 3% BSA (Sigma-Aldrich) and 0.5% Triton X-100 (Sigma-Aldrich). APE1 was detected using anti-APE1 antibody (sc-17774, Santa Cruz Biotechnology) followed by donkey anti-mouse Alexa 568 antibody (#A10037, Thermo Fisher). Follicles were identified using anti-human IgD-FITC antibody (#555778, BD Biosciences). Cell nuclei were counterstained using DAPI (supplemented in mounting media). Stained sections were mounted using Vectashield antifade mounting medium (#H-1000 or #H-1200, Vector Laboratories) and visualized using an Olympus IX71 inverted fluorescence microscope or a Zeiss Axio ScanZ1. Images were compiled using Photoshop CS6 software.

In vitro B cell cultures

Flow cytometry purified human tonsil B cells were cultured in complete media: RPMI 1640 media (Sigma-Aldrich) supplemented with 2 mM L-Glutamine (GIBCO), 100 U penicillin-streptomycin (GIBCO), 0.1 mM nonessential amino acids (GIBCO), 100 mM HEPES (GIBCO), 55 mM β-mercaptoethanol (GIBCO) and 10% FBS (GIBCO). Cells were maintained for 72 h in an incubator at 37°C with 5% CO_2.

Immunoblot

Naive, DZ and LZ B cells were isolated from human tonsils by flow cytometry. One fraction of naive B cells was stimulated *in vitro* for 72 h with IL-21 (10 ng/mL, #130-094-563, Miltenyi Biotec) and CD40L (1 μg/mL, #310-02, PeproTech). Total protein extraction was performed using RIPA buffer (#89901, Thermo Fisher) supplemented with phosphatase and protease inhibitor (#4906845001 and #11873580001, Roche). 10 μg of whole-cell extracts from each cell subset were separated by SDS-PAGE (12% w/v), blotted onto nitro-cellulose membranes and incubated with anti-APE1 antibody (sc-17774, Santa Cruz Biotechnology). β-actin was used as a loading control (#A5441, Sigma-Aldrich). Enhanced chemiluminescence (ECL) development was performed after incubation with secondary antibodies conjugated to horseradish peroxidase (HRP) using Clarity Western ECL Substrate (#1705061, Bio-Rad) according to manufacturer's instructions. Images were acquired on an Image Quant LAS 4000 machine (GE Healthcare Life Sciences). Densitometry analysis was performed using Image Studio software version 5.2.5 (LI-COR Biosciences).

qPCR analysis

Total RNA was extracted from mouse samples with Trizol (#15596026, Thermo Fisher). RNA quality and concentration were determined with an Agilent 2100 Bioanalyzer instrument. Only samples with a RIN score over 8 were selected for DNA digestion and cDNA synthesis using RQ1 RNase-Free DNase (#M6101, Promega) and SuperScript III Reverse Transcriptase (#18080093, Thermo Fisher), respectively. Duplex qPCR analyses were conducted for each target gene (FAM-labeled probe sets) using *Ubc* (VIC-labeled, Taqman assay #Mm01198158_m1, Thermo Fisher) or *Actb* (HEX-labeled probe set, Biosearch Technologies) as reference genes. Samples were measured in triplicate using TaqMan Gene Expression Master Mix (#4369016, Thermo Fisher) in an Applied Biosystems 7900HT Fast Real-Time machine (Thermo Fisher) with the following thermocycler condition: 50°C for 2 min (1 cycle); 95°C for 10 min (1 cycle); 40 cycles of 95°C for 15 s and 60°C for 1 min. Sequences of primers and dual-labeled BHQ probes used to detect GLTs are listed in Table S1. These assays have been previously described (Marshall et al., 2011) and were manufactured by Biosearch Technologies. Data is expressed as a fold-change using the $\Delta\Delta C_T$ method.

One step qPCR analysis

Total RNA from 2,000-15,000 cells was purified using a PicoPure RNA Isolation Kit (#KIT0204, Thermo Fisher) according to the manufacturer's instructions. DNase treatment was performed on-column using RNase-Free DNase Set (#79254, QIAGEN). Quality and concentration were determined as previously described using an Agilent 2100 Bioanalyzer instrument. Real-time one-step RT-PCR quantification was performed using the QuantiTect Multiplex RT-PCR Kit (#204643, QIAGEN) in a final volume of 6 μL. Duplex reactions with limiting primer concentrations were conducted in the same well for *γ1-GLT* (FAM-labeled probe set) and *Actb* (HEX-labeled probe set). Reactions were run in an Applied Biosystems 7900HT Fast Real-Time machine with the following thermocycler condition: 50°C for 20 min (1 cycle); 95°C for 15 min (1 cycle); 40 cycles of 94°C for 45 s and 60°C for 45 s. Expression of the target genes was normalized using the reference gene *Actb* and presented as a fold-change using the $\Delta\Delta C_T$ method.

Single cell qPCR

Single cell qPCR was performed as previously described (Nefzger et al., 2016). In brief, cells were flow cytometry deposited into qPCR 96-well plates filled with 10 μL of lysis buffer and processed with the Single Cell to C_T kit (#4458236, Thermo Fisher). cDNA was produced from the lysate as per kit's instructions. Samples were submitted to 18 cycles of pre-amplification using the following TaqMan assays (Thermo Fisher): *Actb* (Mm00607939_s1), *Foxo1* (Mm00490672_m1), *c-Myc* (Mm00487804_m1), *Apex1* (Mm01319526_g1), *Apex2* (Mm00518685_m1), *Prdm1* (Mm00476128_m1), *Bcl6* (Mm00477633_m1), *Aicda* (Mm01184115_m1), *Cxcr4* (Mm01292123_m1), and *Cd86* (Mm00444543_m1). GLTs were detected using custom probe sets (see Table S1). Single cell qPCR data collection was performed with a Biomark instrument (Fluidigm) on pre-amplified templates that were positive screened for the housekeeper *Actb* (manually tested by qPCR). Reactions were run for 40 cycles. Data was analyzed using the Biomark software package ''Real-Time PCR analysis'' (Fluidigm). Data cleaning and normalization were done using custom R code (R version 3.3.3, R Core Team). The limit of detection was set to 40 cycles. Undetermined C_T were given a value of 40. Heatmaps and violin plots of the resulting data were generated using the ggplot2 package (version 2.2.1) in the R environment.

GC B cell clonal trees from GFP-photoactivatable (GFP-PA)-transgenic mice

GFP-PA-transgenic mice (Victora et al., 2010) were immunized with CGG-alum and draining popliteal lymph nodes (pLNs) were harvested 15 and 20 days later. Two individual GCs per pLN were photoactivated and single-cell sorted independently. Heavy-chain variable-segment (V_H) genes from individual B cells were amplified, sequenced and analyzed as described previously (Tas et al., 2016). Briefly, single cells were lysed in TCL buffer (QIAGEN) with 1% β-mercaptoethanol. SPRI bead isolated RNA was reverse-transcribed into cDNA using an oligo(dT) primer. *Igh* and *Igk* transcripts were amplified from cDNA by PCR. Single-cell barcoded PCR amplicons were sequenced using the MiSeq platform (Illumina, MiSeq Reagent Nano Kit v2). Ig heavy variable (V), diversity (D) and joining (J) gene segments were assigned using the IMGT (Lefranc et al., 2009) and VBASE2 (Retter et al., 2005) databases. Functional V(D)J sequences were grouped into clones only when sharing *Ighv* and *Ighj* gene segments and junction regions (identical length and more than 75% amino acid identity in CDR3). Data for day 15 was re-analyzed from published sequences (Tas et al., 2016) using a similar methodology, and data for day 20 was generated *de novo* for this study. Only clones containing $\geq$ 3 IgM^+ cells, or at least one IgM^+ and one IgG^+ cell, were considered informative and are presented in this paper. Clonal phylogenies and trees were constructed by the inference methodology algorithm GCtree (DeWitt et al., 2018).

Using AID-Cre-Confetti mice to track Peyer's Patch GCs

AID-Cre-Confetti mice (Tas et al., 2016) were used to visualize and track single GCs in the follicles of Peyer's Patches (PPs) of unimmunized mice. In these mice, upon the administration of tamoxifen, AID-expressing GC B cells are marked with one of ten fluorescent color combinations. In order to induced Cre-mediated recombination, 10 mg of tamoxifen in corn oil was administered twice by oral gavage two days apart. PP's were analyzed 18 days after the final administration of tamoxifen. Single PP's were isolated from the entire length of the small intestine and imaged with two-photon microscopy to locate single GC follicles. Individual GCs were then isolated by manual dissection prior to single-cell sorting. Following sorting, single cells were processed for sequencing as previously described.

Nojima cell co-cultures

Co-cultures using the Nojima feeder cells were conducted as previously described (Nojima et al., 2011). Spleens were collected from C57BL/6 wild type mice and naive B cells were magnetically purified using a B cell isolation kit (#130-090-862, Miltenyi Biotec) according to manufacture's instructions. The purified B cells were labeled with Cell Trace Violet (CTV) (#C34571, Thermo Fisher) according to manufacturer's instructions, and then co-cultured for 72 h with Nojima feeder cells in complete media supplemented with recombinant murine IL-4 (10 ng/μL, #214-14, PeproTech). These *in vitro* derived GC (iGC) B cells were flow cytometry-purified to assess binding of BCL6 to the *γ1-GLT* promoter by chromatin immunoprecipitation (ChIP).

Chromatin immunoprecipitation (ChIP)-qPCR

ChIP-qPCR experiments were conducted as previously described (Kagey et al., 2010). Briefly, iGC B cells were flow cytometry-purified and then cross-linked with 1% formaldehyde for 10 min at room temperature, after which glycine was added to stop the reaction. Cells were washed three times with PBS 1x at 4°C, lysed with SDS-lysis buffer (1% SDS, 10 mM EDTA, 50 mM Tris-HCl pH 8) on ice for 10 min. Chromatin was sonicated using a Bioruptor instrument (Diagenode) to generate DNA fragments of 300-1000bp. Anti-Bcl6 (sc-858, Santa Cruz) antibody was used for ChIP. Amplification of ChIP DNA was performed using Power SYBR Green PCR Master Mix (#204643, Thermo Fisher) in a 7900HT Fast Real-Time machine (Thermo Fisher). qPCR reactions were performed in duplicate with the following thermocycler condition: 50°C for 2 min (1 cycle); 95°C for 10 min (1 cycle); 40 cycles of 95°C for 15 s and 60°C for 1 min. ChIP-qPCR data was normalized using the percent input method 2^(average C_T input – average C_T IP sample) (Thermo Fisher). Primer sets used for ChIP-qPCR experiments are listed in Table S2.

Bioinformatic analysis of ChIP-on-chip datasets and prediction of BCL6-binding sites in GLTs

Using ChIP-on-chip data (Ci et al., 2009) of BCL6 gene targets in human GC B cells, the APEX1 and APEX2 loci were analyzed for BCL6 binding peaks as previously described (Ci et al., 2009). The known BCL6 targets *TLR1* and *BCL6* were used as controls. The

dataset was obtained from the Gene Expression Omnibus (GEO) database, accession number GSE15179. BCL6 binding sites in the *γ1-GLT* promoter were predicted using the JASPAR 2018 database (Khan et al., 2018).

QUANTIFICATION AND STATISTICAL ANALYSIS

Datasets were analyzed using Mann-Whitney test (U test, two-tailed), except for quantification of western blots, in which a paired t test (two-tailed) was used. To compare more than two groups or sets of data a Kruskal-Wallis test was performed followed by Dunn's post-test. The test employed to analyze the different experiments is indicated in each figure legend. Statistical tests were selected based on the distribution and the variance characteristics of the data. Normality was assessed with Shapiro-Wilk test. All statistical analyzes were performed with Prism software version 7 (GraphPad Software) and R software version 3.3.3 (The R Foundation for Statistical Computing). The exact *p-value*s are shown in each figure.

Mathematical modeling

All simulations are based on a previously published agent-based model of B and T cell dynamics within the GC (Meyer-Hermann et al., 2012), which lacks an isotype switching model (see below). Briefly, the model describes dynamics of B and T cells in discrete three-dimensional space including diffusion of chemotactic signals that influence cell motility. The GC reaction starts with founder B cells migrating into the virtual GC area within the first four days at a rate of 2 cells per h (of note, the B cell influx was prolonged in Figure S7A). Each B cell divides six times before it is allowed to differentiate to a LZ phenotype that depends on antigen collection for survival beyond a critical time period. Antigen is collected by B cells in an affinity-dependent manner, where affinity of a B cell for an antigen is represented by Hamming distance in four-dimensional shape space. Furthermore, B cells depend on T cell help for survival. For competing B cells, T follicular helper (T_{FH}) cells polarize toward the cell with the higher amounts of collected and processed antigen. B cells collect T_{FH} signals and require a sufficient total amount of collected signal for survival. Each selected B cell returns to the DZ and divides a number of times that depends on the amount of collected antigen, a mechanism termed dynamic number of divisions (Meyer-Hermann, 2014) and supported by experimental data (Gitlin et al., 2014). Differentiation to GC output cells is induced in a probabilistic manner (LEDAX model) (Meyer-Hermann et al., 2012). A full description of the modeling framework and its compatibility with recent experimental data has been recently published (Binder and Meyer-Hermann, 2016).

For the present context of B cell isotype switching, a new model of GC dynamics needed to be developed, which explicitly represents the different isotypes and allows for different models of how isotype switching happens. Newly arrived cells are assumed to predominantly express IgM. In accordance with early measurements of the amount of IgG^+ B cells (Figures 1C and 2A–2D), we assume that 35% of the founder cells are already expressing IgG. At each division event, the daughter cells switch from IgM to IgG with a defined probability. This switching probability p can be either constant or decrease over time according to an exponential decay model with a half-life corresponding to the observed decrease in GLTs (Figure 1E), $p(t) = p_0\, e^{-\gamma t}$, where p_0 denotes the switching probability at the beginning and γ is the decay of the switching probability over time. The initial switching probability is not a free parameter, this was determined by data on the relative amount of either isotype at later time points of the reaction in Figures 4F and 4G for both the constant (p = 0.03 at each division, unless stated otherwise) and the dynamic (p_0 = 0.15 at each division) switching model separately.

To account for a possible preferential output for the IgG isotype, we introduced a bias factor, η, that increases the probability for IgG^+ cells to become plasma cells while decreasing the output probability for IgM^+ cells by the same amount, keeping the total amount of output cells comparable. The different conditions were simulated in 400 *in silico* GCs and the distribution of the fraction of IgG^+ B cells at day 21 after onset of the GC reaction was evaluated among these 400 GCs.

To test for the impact of the timing of CSR, we combined the dynamic switching model with a delay in switching, leading to a limited time interval for switching at different times of the GC reaction. We tested a delay of different time intervals, t_{switch} (Figure 5G). Each delay was simulated in 400 GCs and the diversity of the IgG fraction at day 21 within these 400 simulations was assessed using the difference between the upper and the lower quartile (interquartile range, IQR).

All simulations were performed using custom C++ code. Simulation output was analyzed using the R statistics language; plots of the simulation output were created using the ggplot2 library.

DATA AND CODE AVAILABILITY

Data, code and materials used in this study can be made available upon request to the corresponding author.